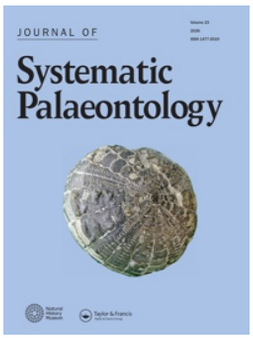

Journal of Systematic Palaeontology

ISSN: 1477-2019 (Print) 1478-0941 (Online) Journal homepage: www.tandfonline.com/journals/tjsp20

A new titanosauriform with European affinities in the Early Cretaceous of Brazil: insights on Somphospondyli phylogeny, histology and biogeography

Elver L. Mayer, Julian C. G. Silva Junior, Leonardo R. Kerber, Bruno A. Navarro, Kamila L. N. Bandeira, Juan C. Cisneros, Eliane P. Sousa, Agostina A. Pereira, Manuel A. Medeiros, Rafael M. Lindoso, Francisco Pedro Cavalcanti Neto, Aline M. Ghilardi, Tito Aureliano, Pedro L. Godoy, Gabriel S. Ferreira & Max C. Langer

To cite this article: Elver L. Mayer, Julian C. G. Silva Junior, Leonardo R. Kerber, Bruno A. Navarro, Kamila L. N. Bandeira, Juan C. Cisneros, Eliane P. Sousa, Agostina A. Pereira, Manuel A. Medeiros, Rafael M. Lindoso, Francisco Pedro Cavalcanti Neto, Aline M. Ghilardi, Tito Aureliano, Pedro L. Godoy, Gabriel S. Ferreira & Max C. Langer (2026) A new titanosauriform with European affinities in the Early Cretaceous of Brazil: insights on Somphospondyli phylogeny, histology and biogeography, Journal of Systematic Palaeontology, 24:1, 2601579, DOI: 10.1080/14772019.2025.2601579

To link to this article: https://doi.org/10.1080/14772019.2025.2601579

Journal of Systematic Palaeontology, 2026
Vol. 24, No. 1, 2601579
http://dx.doi.org/10.1080/14772019.2025.2601579

A new titanosauriform with European affinities in the Early Cretaceous of Brazil: insights on Somphospondyli phylogeny, histology and biogeography

Elver L. Mayer[a], Julian C. G. Silva Junior[b], Leonardo R. Kerber[c], Bruno A. Navarro[d], Kamila L. N. Bandeira[e], Juan C. Cisneros[f], Eliane P. Sousa[g], Agostina A. Pereira[h], Manuel A. Medeiros[i], Rafael M. Lindoso[j], Francisco Pedro Cavalcanti Neto[k], Aline M. Ghilardi[l], Tito Aureliano[l], Pedro L. Godoy[m], Gabriel S. Ferreira[n] and Max C. Langer[o]*

[a]Colegiado de Geologia, Universidade Federal do Vale do São Francisco, Av. Tomaz Guimarães s/n, 48.970-000, Senhor do Bonfim-BA, Brazil; [b]Faculdade de Engenharia de Ilha Solteria, Universidade Estadual Paulista, R. Monção 830, 15385-000, Ilha Solteira-SP, Brazil; [c]Centro de Apoio à Pesquisa Paleontológica da Quarta Colônia, Universidade Federal de Santa Maria, R. Maximiliano Vizzoto 598, 97.230-000, São João do Polêsine-RS, Brazil; [d]Laboratório de Paleontologia e Herpetologia, Museu de Zoologia, Universidade de São Paulo, Av. Nazaré 481, 04263-000, São Paulo-SP, Brazil; [e]Laboratório de Sistemática e Biogeografia, Departamento de Zoologia, Instituto de Biologia Roberto Alcântara Gomes, Universidade do Estado do Rio de Janeiro, Rua São Francisco Xavier 524, 20550-013, Rio de Janeiro-RJ, Brazil; [f]Museu de Arqueologia e Paleontologia, Universidade Federal do Piauí, Ininga, 64049-550, Teresina-PI, Brazil; [g]Departamento de Biologia, Universidade Estadual do Maranhão, Av. Oeste Externa 2220, 65055-970, São Luís-MA, Brazil; [h]Centro de Pesquisa de História Natural e Arqueologia do Maranhão, R. do Giz 59, 65010-680, São Luís-MA, Brazil; [i]Universidade Federal do Maranhão, Av. dos Portugueses s/n, 65085-580, São Luís-MA, Brazil; [j]Instituto Federal de Educação, Ciência e Tecnologia do Maranhão, Av. Getúlio Vargas 04, 65.030-005, São Luís-MA, Brazil; [k]Geoactiva Gestão Mineral e Planejamento Ambiental LTDA, Av. Newton Bello S/N, 65919-050, Imperatriz-MA, Brazil; [l]Diversity, Ichnology and Osteohistology Research Group (DINOlab), Universidade Federal do Rio Grande do Norte, R. das Engenharias s/n, 59078-970, Natal-RN, Brazil; [m]Departamento de Zoologia, Instituto de Biociências, Universidade de São Paulo, R. do Matão 321, 05508-090, São Paulo-SP, Brazil; [n]Senckenberg Centre for Human Evolution and Palaeoenvironment, University of Tübingen, Hölderlinstraße 12, 72074, Tübingen, Germany; [o]Departamento de Biologia, FFCLRP, Universidade de São Paulo, Av. Bandeirantes, 3900, 14.040-901 Ribeirão Preto-SP, Brazil

(Received 25 June 2025; accepted 3 November 2025)

A non-titanosaur Somphospondyli specimen unearthed from Early Cretaceous (Aptian) deposits of north-eastern Brazil allowed the establishment of a new taxon, *Dasosaurus tocantinensis* gen. et sp. nov. Shared synapomorphic traits, notably a complex of three anteroposteriorly elongated ridges in the middle and posterior caudal vertebrae, with a groove above the ventral one, and a well-developed lateral bulge on the femur, support the position of the new sauropod as sister to *Garumbatitan morellensis*, from the Barremian of Spain. Osteohistological patterns recognized in *D. tocantinensis* include a mixture of traits previously recognized separately in early diverging neosauropods and later titanosaurs, including an external fundamental system and remains of primary laminar tissue, along with a high degree of secondary remodelling. Apart from expanding the known diversity of Early Cretaceous sauropods in the northern part of South America, this discovery highlights biogeographical connections with more northern Gondwanan areas, as well as Europe. In fact, numerical biogeographical analyses suggest that the clade formed by *D. tocantinensis* and *Ga. morellensis* had a European origin, with the lineage including *D. tocantinensis* dispersing to South America via northern Africa at some point between the Valanginian and Aptian.

https://zoobank.org/urn:lsid:zoobank.org:pub:0BF20DD1-159D-40EE-8E46-3EE88771470A

Keywords: Cretaceous; Somphospondyli; biogeography; Sauropoda; *Dasosaurus*

Introduction

Somphospondyli Wilson & Sereno, 1998, is the maximal clade containing *Saltasaurus loricatus*, but not *Giraffatitan brancai* (Silva Junior et al., 2022). Recent studies have assigned a broad array of non-titanosaur sauropods to this clade, widespread across Europe, Asia, South and North America, Africa, and Australia, spanning in age from the Berriasian to the Santonian (Carballido, Bellardini, et al., 2022; Mocho et al., 2023), with possible Late Jurassic records (e.g. Mannion et al., 2013; Mannion, Upchurch, Schwarz, et al., 2019). Instead, most somphospondyls recorded in Brazil belong to Titanosauria and come from Late Cretaceous

*Corresponding author. Email: langer.mc@gmail.com

Published online 12 Feb 2026

deposits, especially the Bauru Basin in the south-eastern part of the country (Langer et al., 2022). However, newly unearthed (e.g. Carvalho et al., 2017; Castro et al., 2007; Ghilardi et al., 2016; Pereira et al., 2024) and recovered historical (Bandeira et al., 2024) specimens, along with long known and new ichnological data (e.g. Carvalho, 2004; Gomes et al., 2024; Leonardi, 1989, 1994), are revealing a relevant Early Cretaceous diversity of Titanosauriforms in the north-eastern part of the country. This is enhanced here with the record of a new, non-titanosaur species of the clade, excavated from Aptian deposits of the Parnaíba Tectonic Province. Its phylogenetic position, sister to *Garumbatitan morellensis*, from the Arcillas de Morella Formation, late Barremian of Spain (Mocho et al., 2023), highlights the close biogeographical connections between north-eastern South America and more northern Gondwanan areas, as well as Europe, towards the end of the Early Cretaceous.

Titanosaurs had the highest rates of bone recycling known among tetrapods (Curry-Rogers & Kulik, 2018; Mitchell & Sander, 2014; Navarro et al., 2022; Stein et al., 2010). Such high rates were absent in brachiosaurids (Klein & Sander, 2008; Mitchell & Sander, 2014; Sander, 2000; Sander et al., 2006), but because most sampled titanosaurs are from the Late Cretaceous, it is currently unknown at which point in time and in which part of the titanosauriform phylogeny such extensive bone remodelling originated. Osteohistological studies conducted here on the new Brazilian species help bridge that evolutionary gap.

Excavation and geological setting

The fossils dealt with here were first identified by archaeologist Daniel Ribeiro da Silva, who spotted them emerging from the base of an approximately 8 m high slope of a road-rail cut in Davinópolis, Maranhão (MA), north-eastern Brazil. The field campaigns were reported to the Agência Nacional de Mineração (ANM) under protocol numbers 015.2021 and 023.2021, in accordance with Brazilian regulations for fossil collection. The specimens were excavated by a team led by ELM and LRK, using 1×1 m quadrants at the site to record the spatial distribution of the fossils and other taphonomic parameters. Photographical and videographical documentation of the excavation was also conducted. The high clay content and plasticity of the bearing rock was such that, when exposed, the matrix dried out and contracted, breaking apart into clumps around the fossils. Most of the fossils were robust enough to be collected without large amounts of rock around them, whereas others required extraction with the use of plaster jackets, due to their fragility or position relative to adjacent remains. The fossils were dispersed over an area of *c*. 6 m^2, mostly clustered towards the northern part of the excavation (Fig. 1).

The site that yielded the new sauropod is set near the south-western border of the Grajaú Basin as defined by Rossetti and Truckenbrodt (1997; see also Ferreira et al., 2021; Pedrão et al., 2002; Rezende, 2002; Rossetti et al., 2001), one of the sub-basins into which the Parnaíba Tectonic Province (Almeida, 1977; Almeida et al., 1981) has been divided (Góes, 1995; Góes & Coimbra, 1996; Góes & Rossetti, 2001). Recent regional geological maps (Costa Neto et al., 2014; Klein & Sousa, 2012) place the site into the exposure area of the Codó Formation (Fig. 2). In the eastern part of the basin, deposits usually referred to that unit were split in two sequences, separated by an erosional disconformity (Mendes & Borghi, 2004; Rossetti et al., 2001). The lower sequence corresponds to the 'typical' Codó Formation, including shales and limestones, deposited in a lacustrine-evaporitic context; the fossil record of which suggests a late Aptian age (Antonioli, 2001; Guerra-Sommer et al., 2021; Ramos et al., 2006; Lindoso & Carvalho, 2012; Lindoso et al., 2016). In the Tocantins River area, where the new fossils were found (Fig. 2), Costa Neto et al. (2014) divided the Codó Formation in three facies associations, from base to top: (1) dark grey shale with limestone intercalations; (2) greenish-grey siltstone with subordinate shale and calciferous sandstone; (3) fine, light greenish-grey calciferous sandstone, with shale and siltstone intercalations. The sediments bearing the new fossils better match facies associations 2 and 3, as well as the coarser 'upper sequence' of Rossetti et al. (2001). As previously proposed by Leite et al. (1975), Rossetti et al. (2001) suggested the correlation of that sequence to the 'Unnamed Unit' or the Alcantara Formation (Anaisse Júnior et al., 2001; Rossetti & Truckenbrodt, 1997), within the Itapecuru Group of Rossetti and Truckenbrodt (1997), São Luís-Grajaú Basin.

The lithology of the site, on the other hand, is more reminiscent of the Itapecuru Formation (see below), particularly as exposed in the Querru Outcrop, at the north-eastern part of the basin (Ferreira et al., 2016). It includes flat parallel beddings of very friable clayish/sandy siltstones and fine yellowish/reddish sandstones, intercalated with more consolidated greyish muddy sandstones, with incipient carbonate cementation and concretions. Bioturbation structures are present, as well as ferruginous coverings of the hematite/goethite type; all laid above an erosional contact with the Grajaú Formation. Hence, the fossil site most likely exposes the lower portion of the Itapecuru Formation amid a more general incidence of the Codó Formation, which occurs

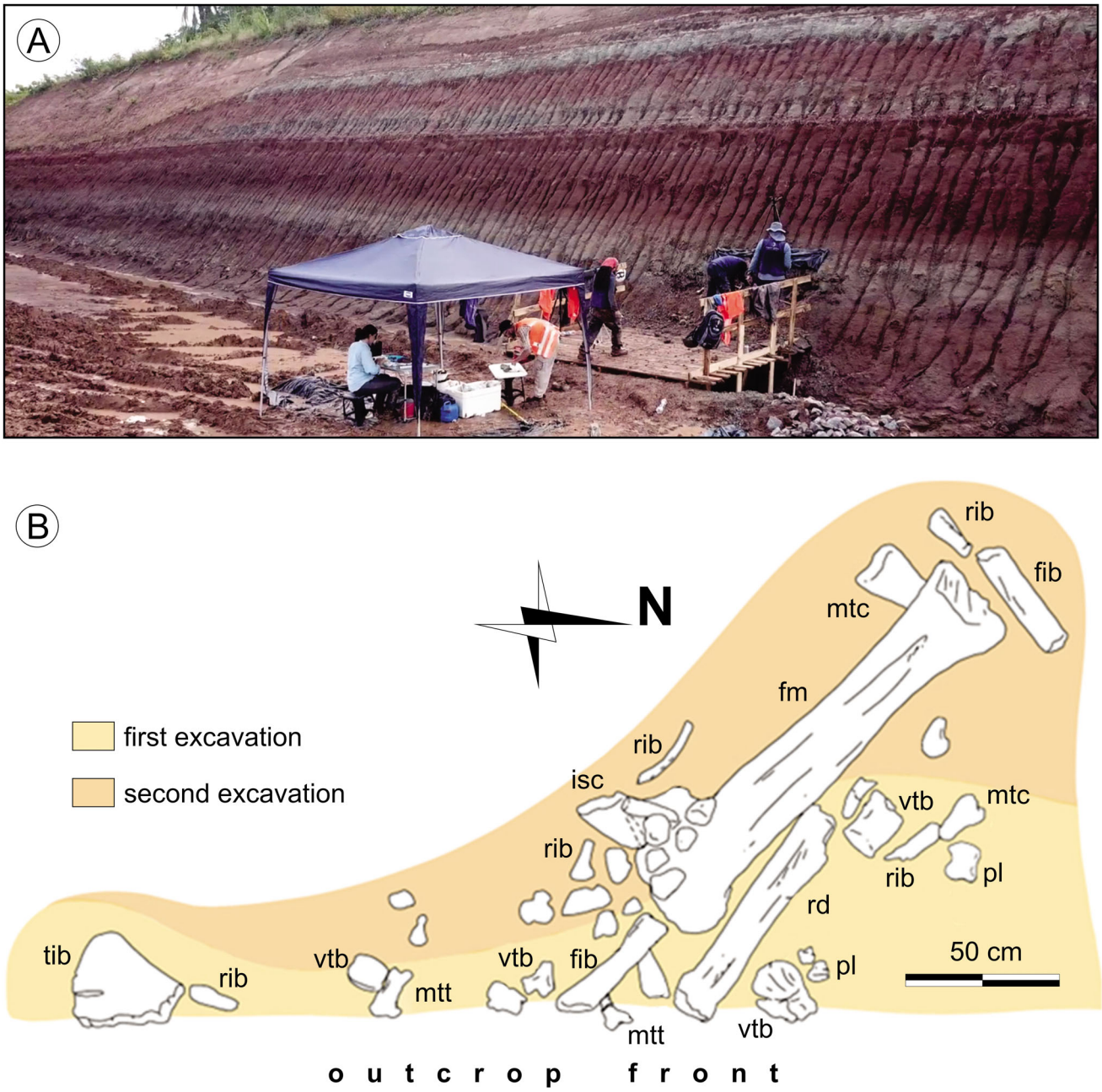

Figure 1. Outcrop view and spatial distribution of fossils in the site. **A,** Photograph of the front of the outcrop. **B,** Horizontal distribution of *in situ* fossils as they were discovered. **Abbreviations**: **fib**, fibula; **fm**, femur; **isc**, ischium; **mtc**, metacarpal; **mtt**, metatarsal; **pl**, phalanx; **rd**, radius; **rib**, rib; **tib**, tibia; **vtb**, vertebra.

in the area as red-brownish fine sandstones, with zeolites remobilized from the CAMP (Central Atlantic Magmatic Province) Mosquito basalts (Merle et al., 2011; Vaz et al., 2007). Enclaves of the Itapecuru Formation seem to be common in the area; see purple areas in Figure 2, corresponding to the 'Varjão Formation' of Costa Neto et al. (2014). In any case, further studies are needed to better place the fossil bearing beds into the stratigraphical and chronological frameworks of the Parnaíba Tectonic Province.

First described as 'Itapecuru Layers' (Lisboa, 1914), and later as a Formation (Campbell, 1949), from outcrops on the banks of the Itapecuru and Alpercatas rivers, more recent accounts (e.g. Corrêa-Martins, 2019; Ferreira et al., 2021; Pedrão et al., 2002; Vaz et al., 2007) have agreed upon a Formation, rather than Group

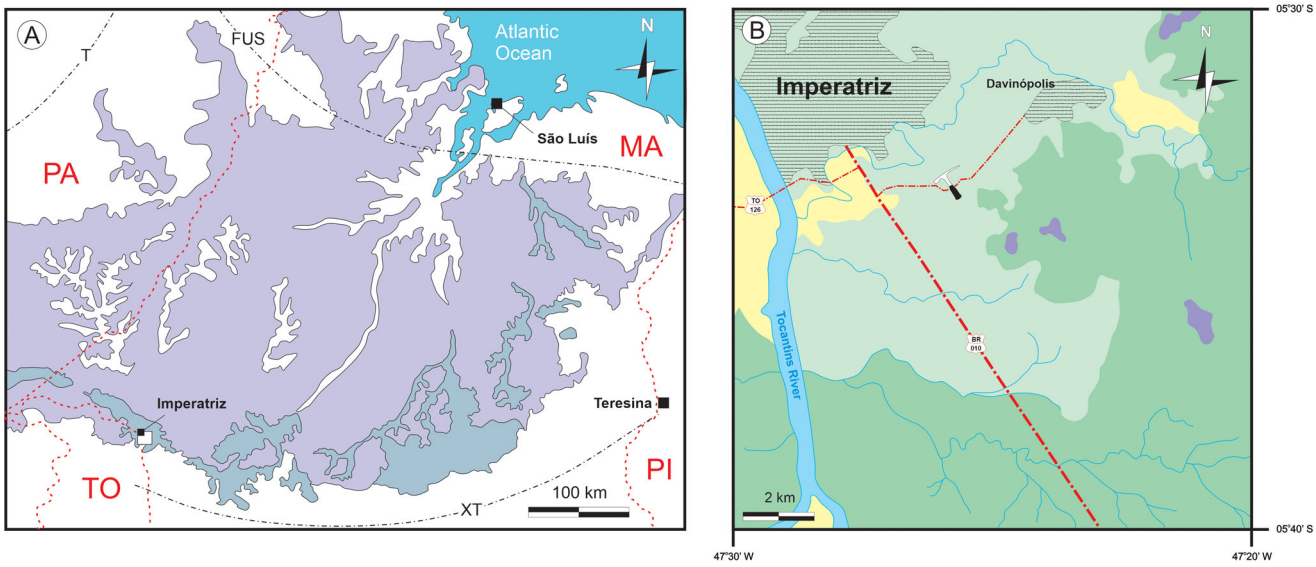

Figure 2. Site location and surface distribution maps of the studied area. **A,** Northern part of the Parnaíba Tectonic Province, showing the distribution of the Itapecuru (purple), Codó, and Grajaú (grey) formations and the main structural borders of the Grajaú Basin, i.e. Tocantins (T), Xambioá-Teresina (XT), and Ferrer-Urbano Santos (FUS) arches; based on Góes and Roseti (2001), Santos and Carvalho (2009), and Ferreira et al. (2021). **B,** Area south-east of Imperatriz highlighted in 'A', based on Costa Neto et al. (2014), showing the digging site (hammer), main roads (red), water courses (blue), urban areas (hatched), and the surface distribution of the Codó (light green), Grajaú (dark green), and Itapecuru (purple) formations, as well as that of Cenozoic deposits (yellow). **Abbreviations**: **MA**, Maranhão state; **PA**, Pará state; **PI**, Piauí state; **TO**, Tocantins state. Red dotted lines in 'A' indicate state limits.

status for that geological unit, which is broadly distributed (Fig. 2) over the Parnaíba Tectonic Province (Corrêa-Martins, 2019; Klein & Sousa, 2012; Mesner & Wooldridge, 1964, Rossetti & Truckenbrodt, 1997). It corresponds to siliciclastic deposits usually composed of reddish and greyish mudstones, siltstones and shales, also exhibiting fine to very fine clayish sandstones and eventually medium to coarse sandstones, conglomerates and limestone levels, interpreted as fluvial, shallow lake, estuarine and deltaic in origin (Corrêa-Martins, 2019; Ferreira et al., 2021; Gonçalves & Carvalho, 1996; Lima et al., 1994; Pessoa & Borghi, 2005; Zalán, 2007).

In a paleoequatorial context of warm semi-arid climate, with marked seasonality and local humid conditions, the Itapecuru Formation bears a noteworthy record of fossil tetrapods, although most remains are found disarticulated and isolated. Dinosaurs are represented by isolated carcharodontosaurid and spinosaurine skeletal remains (Arcanjo et al., 2023; França et al., 2025; Medeiros et al., 2014), and by more abundant sauropod records, including titanosaurs and diplodocoids, such as the rebbachisaurid *Amazonsaurus maranhensis* (Carvalho et al., 2003; Castro et al., 2007; Silva, 2023). Other reptiles include the pleurodire turtle *Itapecuruemys amazonensis* (Batista et al., 2020) and the crocodyliform *Candidodon itapecuruense* (Carvalho, 1994). In terms of age, as reviewed by Ferreira et al. (2020), the fossil record of the Itapecuru Formation indicates a general referral to the Aptian–Albian, but more recently gathered palynological data narrow the age of its lower potion to the late Aptian, at least in the studied outcrops to the eastern portion of the basin (Ferreira et al., 2020).

Material and methods

The fossils were initially housed and prepared at Universidade Federal do Sul e Sudeste do Pará (UNIFESSPA), in São Félix do Xingu-PA, but ultimately deposited at the fossil collections of Centro de Pesquisa de História Natural e Arqueologia do Maranhão (CPHNAM), in São Luis-MA. This is a public repository, in which specimens are kept available for the entire scientific community. Anatomical measurements and phylogenetic definitions can be seen in Supplemental material Tables 1–3. In agreement with article 6, recommendation 6.1A, of the PhyloCode (Cantino & De Queiroz, 2020), all clades established under that code are italicized. For vertebral laminae and fossae terminology, we respectively follow the nomenclature proposed by Wilson (1999, 2012) and Wilson et al. (2011).

Anatomical indices employed here are a follows: average elongation index (aEI) = anteroposterior length of the centrum (excluding the posterior condyle) divided by a mean of its lateromedial width and the dorsoventral height of its posterior articular surface (*sensu* Chure et al., 2010); eccentricity index (EI) = long bone mediolateral width divided by its anteroposterior width at mid-shaft (*sensu* Wilson & Carrano, 1999); robustness index (RI) = maximum proximodistal length of a limb element divided by the mean of its greatest lateromedial widths measured at the proximal end, mid-shaft and distal end (*sensu* Wilson & Upchurch, 2003).

To estimate the body size of the new sauropod, we performed a linear regression analysis in R environment (R Core Team, 2022; Supplemental material file 1), correlating the estimated total body lengths of the exceptionally well-preserved titanosaurs *Rapetosaurus krausei* (Curry-Rogers & Forster, 2001) and *Dreadnoughtus schrani* (Lacovara et al., 2014) with the maximal length (measured along its proximodistal axis) of the preserved femur of CPHNAM VT 1600, based on the corresponding measurement of the same element in those titanosaurs.

The phylogenetic position of the new sauropod was evaluated based on the dataset of Mocho et al. (2023), originally adapted from that of Poropat et al. (2023). As in those analyses, multistate characters (11, 14, 15, 27, 40, 51, 104, 122, 147, 148, 195, 205, 259, 297, 426, 435, 472 and 510) were treated as ordered and eight operational taxonomic units (OTUs) were excluded *a priori* (i.e. *Astrophocaudia slaughteri*, *Australodocus bohetii*, *Brontomerus mcintoshi*, *Fukuititan nipponensis*, *Fusuisaurus zhaoi*, *Liubangosaurus hei*, *Malarguesaurus florenciae* and *Mongolosaurus haplodon*). The new taxon was added to the Mocho et al. (2023) matrix, with its character scores listed in Supplemental material file 4 (available through OSF = The Open Science Framework; Godoy, 2025), and two further OTUs, '*Garumbatitan* holotype' and '*Garumbatitan* paratype', were excluded, because they are already represented in the dataset by the '*Garumbatitan morellensis*' OTU. In addition, based on comparative information, two new characters (chars. 557 and 558) were introduced. The first applies to a complex of three anteroposteriorly elongated ridges seen on the pedicels of the middle and posterior caudal vertebrae, scored as absent (0) or present (1). Note that these ridges are osteological correlates of epaxial and hypaxial muscle insertions, which may vary in development within the caudal series. Also, they might not be described, or not described in detail, for many taxa, so their absence cannot easily be confirmed based on the literature. Likewise, these muscle insertions might occur with different shapes (e.g. ridges, protuberances, rugosities). The second added character corresponds to the lateral expansion of the lateral bulge of the femur in anterior/posterior views (Mocho et al., 2023, fig. 25; Salgado et al., 1997), scored as less than (0), equal to, or more than (1) 40% the minimal transverse width of the shaft. The scores of those two characters for the entire set of OTUs can also be seen in source data file 5, which is available through OSF (Godoy, 2025). The final data matrix includes 558 characters and 119 OTUs – out of the original 128 OTUs of Mocho et al. (2023) – and is available through OSF (source data files 2–3 Godoy, 2025). The dataset was analysed using TNT 1.5 (Goloboff & Catalano, 2016), with *Shunosaurus* as the operational outgroup. We followed the search protocol of Poropat et al. (2021, 2023). A first analysis was conducted selecting the option 'Stabilize Consensus' of the 'New Technology Search', incorporating sectorial searches, ratchet, drift and tree fusing, with the consensus stabilized five times and all other search parameters kept as default. It is worth mentioning that, when using this protocol, users do not need to recalculate the consensus from all most parsimonious trees (MPTs), since the consensus tree is saved in TNT as the last saved tree after running a 'stabilize consensus' analysis, using the tree bisection & reconnection (TBR) algorithm. The first analysis used a reduced version of the data matrix, after excluding two OTUs ('Cloverly titanosauriform' and *Ruyangosaurus giganteus*), following Poropat et al. (2021). The second analysis used the complete matrix (119 OTUs) but was conducted with implied weighting (K-value = 9).

We used the strict consensus that resulted from the parsimony analysis with implied weighting as the phylogenetic framework for our biogeographical analyses. For that, we time-calibrated this consensus topology based on OTU age information (first and last appearances) taken from the literature and the Paleobiology Database (see source data file 4, available through OSF; Godoy, 2025), using the cal3 method (Bapst, 2013), and following scripts kindly made available by Stubbs et al. (2021). To incorporate temporal uncertainties related to imprecise tip ages (i.e. age ranges related to the rocks in which fossils were found), we calibrated 10 versions of this topology (see source data file 5, available through OSF; Godoy, 2025), each of which contained different node ages and branch lengths. Independently for each of the 10 trees, we also randomly resolved the polytomies from the consensus topology, incorporating phylogenetic uncertainty. Ideally, more time-calibrated trees should be used for macroevolutionary analyses (Bapst, 2014; Godoy et al., 2020), but this limited number was used in our study because the biogeographical analyses are very time-consuming. For the cal3 method, three

different rates are needed: sampling, branching (or speciation/origination) and extinction rates. The branching and extinction rates (which we assumed to be the same, following Bapst & Hopkins, 2017) were obtained with the Rate2sProb function from the R package paleotree (Bapst, 2012), dividing them by interval length. The sampling rate is not easily estimated for this type of dataset (full of singletons) and was therefore randomly drawn from a uniform distribution of previously estimated rates for dinosaurs and other tetrapods (Bapst & Hopkins, 2017; Lloyd et al., 2016). The 10 time-calibrated trees were used for subsequent biogeographical analyses.

We ran three stratified biogeographical analyses using the R package BioGeoBEARS (Matzke, 2013, 2014) for each of the 10 trees. The analyses employed dispersal-extinction cladogenesis (DEC; Ree, 2005, Ree & Smith, 2008), likelihood versions of the dispersal-vicariance analysis (DIVALIKE; Ronquist, 1997) and BayArea (BAYAREALIKE; Landis et al., 2013) methods. Each of these methods assumes different models of geographical range evolution (Matzke, 2013) and their implementation in a common likelihood framework in BioGeoBEARS enables model comparison and selection. We considered 10 geographical areas: Appalachia (Ap), Laramidia (La), northern (nSA) and southern (sSA) South America, northern (nAf) and southern (sAf) Africa, Indo-Madagascar (IM), Asia (As), Europe (Eu), and Australasia (Au). Each terminal in the tree was scored for its known distribution and although the maximum observed range is 2, we determined a maximum range size of 4 for the ancestral nodes. Stratification in BioGeoBEARS sections the tree into defined time periods, each of which can have a different dispersal multiplier matrix defined. Depending on the proximity and connectivity between the areas we set an index varying from 0.000001 to 1. The dispersal probability between two areas is multiplied by those matrices, enabling palaeogeographical models to be used in such analyses. We defined those indices by modifying the nine-step model recently proposed by Upchurch and Chiarenza (2024) to also include the relations between northern and southern portions of Africa and South America. We used the Akaike information criterion (AIC; Akaike, 1974) and second-order information criterion (AICC; Sugiura, 1978) to select the best fitted model for each tree. All time-calibration and biogeographical analyses were performed in R v.4.2.2 (R Core Team, 2022); our R code and associated files are available through OSF as source data file 6 (Godoy, 2025).

Samples from the femur and tibia midshafts and a rib fragment were acquired to describe the bone microstructure/histology. Whenever possible, samples were collected along natural breaks; otherwise, they were cut with a saw. The fragments were stabilized with PaleoBOND® PB0020, embedded into Araldite® 2020 resin and ground to a thickness of approximately 60 µm. We analysed and photographed the thin sections using an Olympus BX53-P polarized microscope attached to an Olympus U-TV0.5XC-3 at the Seismology Laboratory (LabSis, UFRN). We followed Francillon-Vieillot et al. (1990) for histological descriptions. High-resolution renders of the osteohistological sections are reposited online on Morphosource (Aureliano, 2025).

Institutional abbreviation

CPHNAM, Centro de Pesquisa de História Natural e Arqueologia do Maranhão, São Luís-MA, Brazil.

Systematic palaeontology

Sauropoda Marsh, 1878
Neosauropoda Bonaparte, 1986
Macronaria Wilson & Sereno, 1998
Titanosauriformes Salgado, Coria & Calvo, 1997 [Silva Junior et al., 2022]
Somphospondyli Wilson & Sereno, 1998 [Silva Junior et al., 2022]
Dasosaurus gen. nov.

Type species. *Dasosaurus tocantinensis* sp. nov., by monotypy.

Etymology. The generic epithet derives from the Greek words δάσος (dásos), meaning forest/copse, and σαῦρος (saûros), meaning lizard/saurian. This refers to the location of the digging site within 'Brazil's Legal Amazonia', a socio-geographical division of the country that includes most of the Amazon rainforest (Nogueira et al., 2018), as well as to a possible origin of the name of the state where the site is located, i.e. Maranhão, which may derive from the Portuguese word 'emaranhado' (= tangled), in reference to the thick vegetation of the area.

Diagnosis. As for the type and only known species.

Dasosaurus tocantinensis sp. nov.
(Figs 3–10, 12–15)

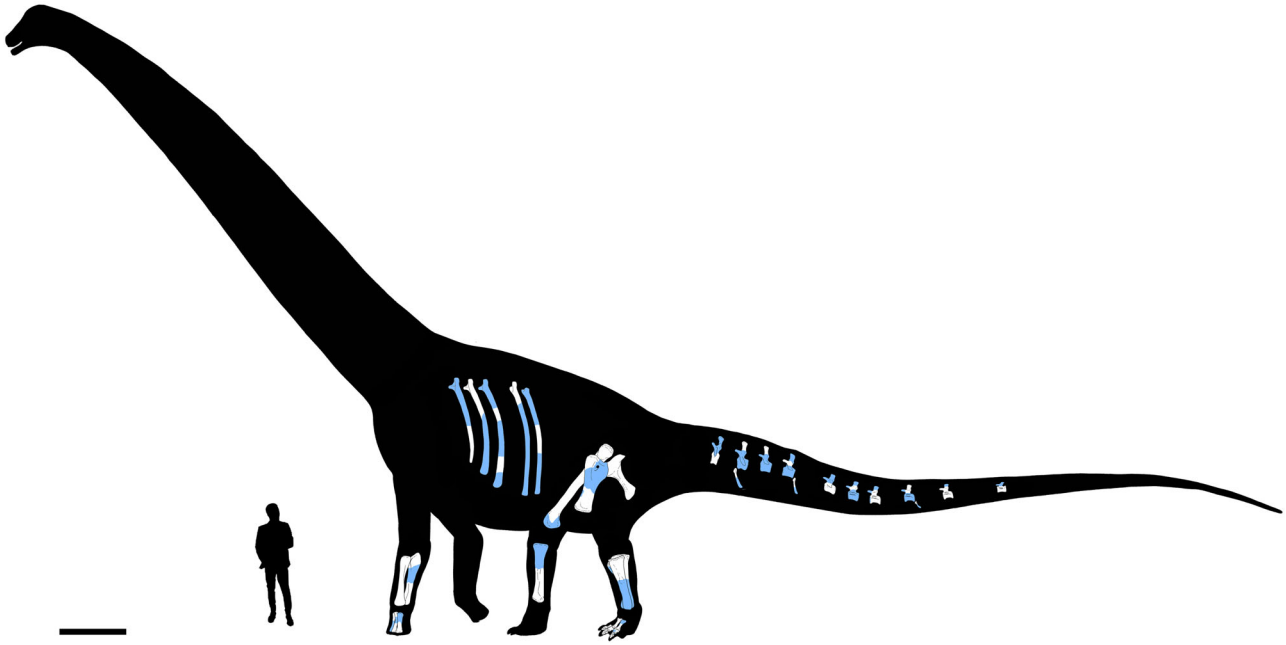

Figure 3. *Dasosaurus tocantinensis* gen. et sp. nov. (CPHNAM VT 1600) Diagrammatic reconstruction with scaled bone elements in anatomical position. Preserved bone portions in white and reconstructed parts in light blue. Human silhouette = 1.80 m. Scale bar = 1 m.

Holotype. CPHNAM VT 1600, partial postcranial remains pertaining to a single individual (Fig. 3), numbered as follows (in parentheses): two anterior caudal centra (1600/1–2); two middle caudal vertebrae (1600/3–4); one posterior caudal centrum (1600/5); four partial anterior caudal neural arches (1600/6–9); four isolated caudal prezygapophyses (1600/10); two isolated anterior caudal neural spines (1600/11–12); four chevron fragments (1600/13); left radius (1600/14); left ulna (1600/15); partial right manus, including a proximal half of a metacarpal II (1600/16), partial metacarpal III (1600/17), and distal half of metacarpal IV (1600/18); distal half of left pubis (1600/19); left ischium (1600/20); right femur (1600/21); proximal ends of left tibia (1600/22) and fibula (1600/23); distal half of right fibula (1600/24); partial left pes, including a complete metatarsal II (1600/25), distal half of metatarsal III (1600/26), non-ungual pedal phalanges I.1 (1600/27), II.1 (1600/28), II.2 (1600/29), III.1 (1600/30), and ungual phalanges I–III (1600/31–33); several trunk rib fragments (1600/34); and other indeterminate bone fragments (1600/35). The femoral dimensions of CPHNAM VT 1600 are comparable to those of the paratype of *Ga. morellensis*, which is significantly smaller than the holotype (Mocho et al., 2023), although osteohistology data (see below) suggests that the individual was already an adult. Based on the classification of González Riga et al. (2022), with a femoral length of at least 150 cm, *D. tocantinensis* falls near the limit between medium (femur length = 110–155 cm) and large (femur length $\geq$ 155 cm) bodied sauropodomorphs. Indeed, the conducted regression indicates a body size of about 20 m for CPHNAM VT 1600 (Supplemental material file 1), although this estimate should be regarded as tentative, given the incomplete preservation of its femur.

Etymology. The species name derives from Tocantins, a major South American river, which also gives its name to the administrative region of the Maranhão state where the new fossils were collected, near the eastern banks of the said river.

Type locality and horizon. The remains of *D. tocantinensis* come from the municipality of Davinópolis-MA, near Imperatriz-MA, Brazil (coordinates: 5°33′25″ S, 47°25′52″ W; Fig. 2), from deposits referred to the lower part of the Itapecuru Formation, late Aptian of the Grajaú Basin (Ferreira et al., 2020, 2021).

Differential diagnosis. *Dasosaurus tocantinensis* can be differentiated from its sister taxon *Ga. morellensis* based on the following unique set of features: (1) dorsal-most of the three neural arch ridges of the middle-posterior caudal vertebrae placed at the level of the dorsal (rather than the ventral) margin of the prezygapophysis and dorsally bounding a shallower, ellipsoid costovertebral concavity; (2) anterior caudal neural spines expanded dorsolaterally (‘stake-like’ shaped), creating a quadrangular dorsal platform; (3) slenderer femur with a more

medially curved shaft; (4) anterior surface of the femur lacking a linea intermuscularis cranialis; (5) less developed lateral bulge on the femur, about 40% of the transverse minimal width of the femoral shaft; (6) pedal ungual phalanges I–II with a dorsolateral extensor tubercle.

In addition, five of the autapomorphies proposed by Mocho et al. (2023) for *Ga. morellensis* are also seen in the Brazilian species (now regarded as synapomorphies of the *Ga. morellensis* plus *D. tocantinensis* clade), helping to differentiate it from other Titanosauriformes, namely: (1) middle to posterior caudal vertebrae pedicels covered by a complex of three anteroposteriorly elongated ridges; (2) middle to posterior caudal vertebrae with a depression above the ventral-most of those three ridges; (3) femur with a well-developed lateral bulge (40% or more of the transverse minimal width of the femoral shaft); (4) laterally deflected and projected proximal tip of the ventrolateral crest of metatarsal II; (5) lateral depression near the dorsolateral ridge of the distal end of pedal phalanx I.1. A sixth synapomorphy of that clade, not included in the diagnosis of *Ga. morellensis*, consists of a sub-rectangular posterolateral process of the tibia (Mocho et al., 2023, fig. 13A, D). Other *Ga. morellensis* autapomorphies proposed by Mocho et al. (2023) are not preserved in the Brazilian species, so that it is unclear if they are unique to the Spanish species or synapomorphies of their clade; these include: (1) middle- to posterior caudal neural spines expanded posteriorly, resulting in lateral rounded boss; (2) metatarsals II–IV more gracile and significantly longer than metatarsals I and V; (3) reduced ungual in pedal digit III. The third pedal ungual of the Brazilian species is also reduced, as commonly seen among neosauropods, but its comparison in length to that of metatarsal III, the parameter proposed by Mocho et al. (2023), is unfeasible because the latter bone is not fully preserved. As for the 'heart-shaped' proximal outline of phalanx II.1, another *Ga. morellensis* autapomorphy proposed by Mocho et al. (2023), this seems to be lacking in the Brazilian species, but possibly due to taphonomic deformation.

Osteological description and comparisons

Axial skeleton. **Trunk ribs.** Several trunk rib fragments (CPHNAM VT 1600/34) were recovered (Fig. 4). They correspond primarily to mid-shaft and distal portions, preserving no meaningful morphology. Their cross-sections vary from sub-rounded to mediolaterally flattened (Fig. 4I), indicating origins from different regions of the trunk series. Among these fragments, some correspond to poorly preserved proximal portions, but lacking most of the capitulum and tuberculum (Fig. 4A–H). They have a crescentic profile in cross-section (Fig. 4J) and the development of an incipient pneumatocoel. However, internal pneumatopores are absent (Fig. 4G).

Caudal vertebrae. These comprise relatively well-preserved vertebral elements, lacking parts of the neural arches, all of which share similar anatomical features and overall morphology. Serial variation in caudal vertebrae was determined following the criteria of Mannion et al. (2013): (1) anterior caudal vertebrae bear ribs, even if reduced; (2) middle caudal vertebrae lack ribs, but retain distinct neural spines and postzygapophyses; (3) posterior caudal vertebrae lack distinct neural spines and postzygapophyses in the neural arches; (4) the posterior-most caudal vertebrae lack well-developed neural arches. Additional comparisons to determine vertebral positions were conducted with macronarians that preserve more complete caudal series, such as *Camarasaurus lentus* (Gilmore, 1925) and *Ruixinia zhangi* (Mo et al., 2023). Based on such comparisons, the described vertebral remains correspond to two centra (CPNHAM VT 1600/1 and 1600/2; Fig. 5A, B), respectively placed more anteriorly and posteriorly along the anterior part of the tail, two complete vertebrae from the middle part of the series (CPNHAM VT 1600/3 and 1600/4; Fig. 5C, D), and one centrum from the posterior portion of the tail (CPNHAM VT 1600/5; Fig. 5E). In addition, several fragmentary remains from other parts of the tail are also present, such as isolated neural spine and chevron portions (CPNHAM VT 1600/6–13; Fig 6). The former elements match in morphology and proportions those of the more completely preserved tail vertebrae and were also attributed to this part of the vertebral column for their nearby association to those elements.

Except for the anterior-most centra, which are amphiplatyan, the remaining centra are amphicoelous, displaying well-concave anterior and posterior articular surfaces, as seen in *Ga. morellensis* (Mocho et al., 2023, fig. 7G). This differs from the less concave surfaces present in *Tastavinsaurus sanzi* (Canudo et al., 2008, fig. 8), as well as from those of *Paluxysaurus jonesi* (Rose, 2007, fig. 16) and *Sauroposeidon proteles* (D'Emic, 2012, fig. 3.9), which bear a lateromedially elongated concavity on their mid-ventral portions. *Dasosaurus tocantinensis* also differs from well-known South American somphospondyls, such as *Chubutisaurus insignis* and *Ligabuesaurus leanzai*, the anterior caudal centra of which are platycoelous and shorter in the anteroposterior axis (Bellardini et al., 2022; Carballido et al., 2011). Furthermore, the vertebrae of *D. tocantinensis* also lack foramina or blind fossae on the lateral surfaces, as well as knobs on the posterior articular facets, conditions shared with *Ga.*

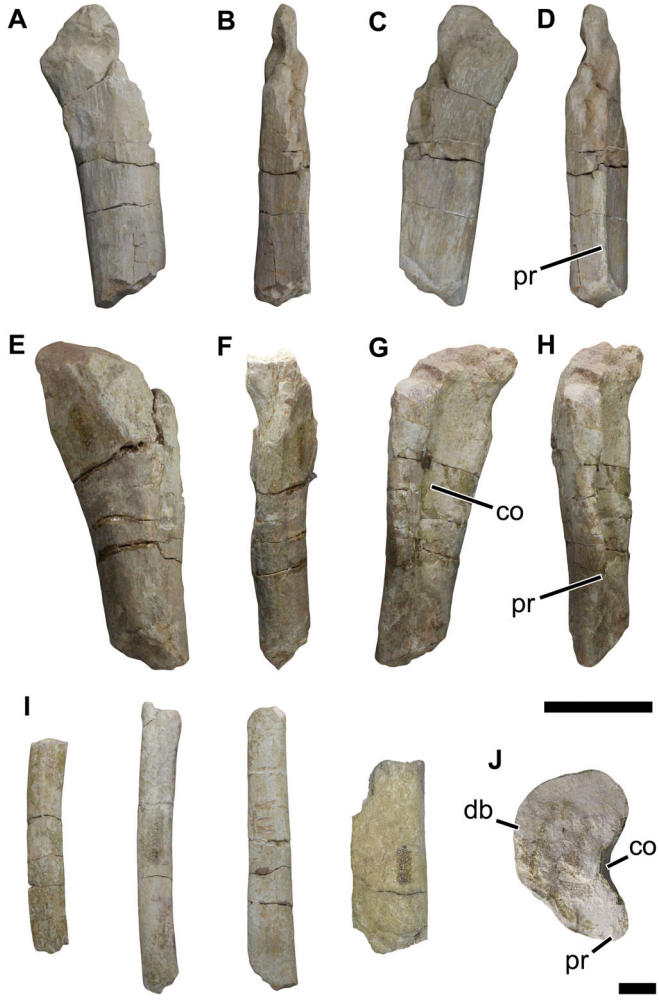

Figure 4. Trunk rib fragments of *Dasosaurus tocantinensis* gen. et sp. nov. (CPHNAM VT 1600/34): proximal end of ribs in **A, E,** anterolateral; **B, F,** medial; **C, G,** posteromedial and **D, H,** posterior views; **I,** some shaft distal segments; **J,** cross-sectional view of proximal end. **Abbreviations**: **co**, coel; **db**, distal bundle; **pr**, posterior ridge. Scale bars = 10 cm (A–I) and 2 cm (J).

morellensis (SAV05-060va, Mocho et al., 2023, fig. 6D) and *T. sanzi* (Canudo et al., 2008, fig. 8). However, it is worth noting that this latter structure may correspond to a pathology, commonly observed in other sauropod caudal vertebrae (e.g. Cruzado-Caballero et al., 2023; Lacerda et al., 2025).

The articular facets for the chevrons are present solely on the posterior margin of the centra. They expand ventrally, face more posteriorly than ventrally, and exhibit a triangular shape in both posterior and lateral views. The anterior-most centrum, although corresponding to the tallest element, is the least elongated, with an aEI of 0.6. In contrast, the centra become more elongated towards the posterior elements, with the remaining centra exhibiting an aEI ranging from 1.1 to 1.5 (Table S1). The lateral and ventral surfaces are slightly concave anteroposteriorly, as more marked in the posterior-most centrum (CPHNAM VT 1600/5).

The lateral surfaces of all vertebrae with a complete neural arch exhibit a complex arrangement of three ridges aligned along the dorsoventral axis for the attachment of the epaxial muscles (Díez Díaz et al., 2020): the dorsal-most at the level of the zygapophyseal base, the middle ridge along the lower margin of the pedicel at the neurocentral joint, and the ventral-most positioned on the dorsal third of the centrum, following the costovertebral line (Fig. 5EE). Between the latter two ridges lies a deep, ellipsoid costovertebral fossa, which no evidence of rib attachment. The dorsal-most ridge is slightly more oblique in the anterior-most vertebra compared to the more horizontal ridge of the following element. Two of those ridges were also described in tail vertebrae of *T. sanzi* (Canudo et al., 2008, fig. 8B), which seem to correspond to the dorsal-most and ventral-most ridges of *Ga. morellensis* and *D. tocantinensis*.

The only preserved prezygapophyses are dorsomedially flattened and long, almost half the centrum length, projecting anterodorsally to surpass the anterior articular facet of the centrum (Fig. 5T). They are connected to one another by an incipient intraprezygapophyseal lamina, which forms the ventral margin of a shallow prespinal fossa, and to the centrum via the centroprezygapophyseal laminae, which are half as laterомedially thick as the neural canal. The prezygapophyseal facets are sub-rounded and dorsomedially projected. The postzygapophyses (Fig. 5O) are short, not reaching the posterior edge of the centrum. Their sub-rounded articular facets face ventrolaterally, forming the medial border of a shallow spinopostzygapophyseal fossa. The postzygapophyses are connected to the centrum via the centropostzygapophyseal laminae, which are gracile and much lateromedially thinner than the neural canal.

The two isolated anterior neural spines (CPHNAM VT 1600/11 and 1600/12) are strongly mediolaterally expanded, giving a 'stake' shape in both anterior and posterior views (Fig 6A, B). The dorsal surfaces are almost flat and bear an incipient sagittal ridge on their posterior portion, forming a dorsal platform for the attachment of the supraspinal ligament (Schwarz-Wings et al., 2009). In addition, the anterodorsal portion of the prespinal lamina is strongly developed, forming a prominent anterior projection. In lateral view, the spinoprezygapophyseal and spinopostzygapophyseal laminae lie vertically, accompanying the margins of the spine. The postspinal lamina is stout and rough, differentiated from the spinopostzygapophyseal laminae by slightly marked grooves, which do not develop into a postspinal fossa.

CPHNAM VT 1600/6 corresponds to a portion of the ventral part of an anterior caudal neural arch (Fig. 6C). The spinoprezygapophyseal laminae extend dorsoventrally, bordering the prespinal fossa, the dorsal part of which is divided into two lateral portions by the prespinal lamina. CPHNAM VT 1600/7 corresponds to a partial neural arch from a middle caudal vertebra, including a portion of its right lateral surface, the neural spine, and the postzygapophyseal articular facets (Fig. 6D). The latter has a sub-rounded outline and leans slightly ventrally. The posterior margin of the postzygapophyses form the lateral border of the spinopostzygapophyseal fossa, which is shallow, set below the dorsoventrally extending postspinal lamina, and ventrally delimited by an intrapostzygapophyseal lamina. The neural spine is thin and anteroposteriorly elongated, lacking the posterodorsal expansion seen in *Ga. morellensis* (Mocho et al., 2023, fig. 7E–J).

Chevrons. Three chevron fragments (CPHNAM VT 1600/13) were preserved. Based on the development of their articular surfaces with the caudal vertebrae, two of them probably correspond to anterior chevrons and one likely represents a more posterior element, based on the development of articular facets (Fig. 7). As in *Ga. morellensis* (Mocho et al., 2023, fig. 7), the haemal processes of the chevrons lack a bony crus connecting them, differing from the condition seen in early eusauropods and euhelopodids (Mannion, Upchurch, Jin, et al., 2019). The articular surfaces are single and subtriangular, separated from the chevron body by an anterior sulcus. They expand laterally, contacting their corresponding vertebra posteriorly, in the same line of the posterior articular surface. Haemal spines were not recovered, preventing any assessment of their morphology or further comparisons.

Appendicular skeleton. **Forelimb.** A left radius (CPHNAM VT 1600/14; Fig. 8G–I) is preserved, lacking its proximal portion. The shaft is mostly straight, arching slightly laterally, and lateromedially compressed. The proximal half (as preserved) bears a subtle concavity in the medial surface and a small proximodistally oriented crest extends along the lateral surface, as in *C. insignis* (Carballido et al., 2011). The mid-shaft cross-section is elliptical, 2.3 times broader lateromedially than anteroposteriorly, differing from the slenderer profile seen in *L. leanzai* (Bellardini et al., 2022). The anterior surface of the proximal portion bears a proximodistally elongated depression, whereas the posterior is mainly flat. The distal surface seems convex, with a slightly bevelled lateral portion. The distal outline is somewhat trapezoidal, with the posterior margin forming a right angle with the straight lateral margin. On the contrary, the distal outline of the radius is subtriangular in some Titanosauriformes, and slightly expanded compared to the shaft, as seen in *T. sanzi* (Royo-Torres et al., 2012), *Cedarosaurus weiskopfae* (Tidwell et al., 1999), and *L. leanzai* (Bellardini et al., 2022).

The preserved left ulna (CPHNAM VT 1600/15; Fig. 8A–F) bears a subtle olecranon process, which projects proximal to the main articular surface. The proximal outline is triradiate, with the anteromedial process hosting a slightly concave humeral articular surface and the anteromedial process sloping distally away from the olecranon in lateral view. The preserved shaft is subtriangular in cross-section and is laterally straight. As in other Titanosauriformes, the posterior ridge is well marked, extending distally from about the estimated mid-length of the bone (Carballido et al., 2011).

The partial right manus includes the proximal half of metacarpal II (CPHNAM VT 1600/16; Fig. 8J–M), a partial metacarpal III (CPHNAM VT 1600/17; Fig. 8N–Q), and the distal half of metacarpal IV (CPHNAM VT 1600/18; Fig. 8R–U). The proximal outline of

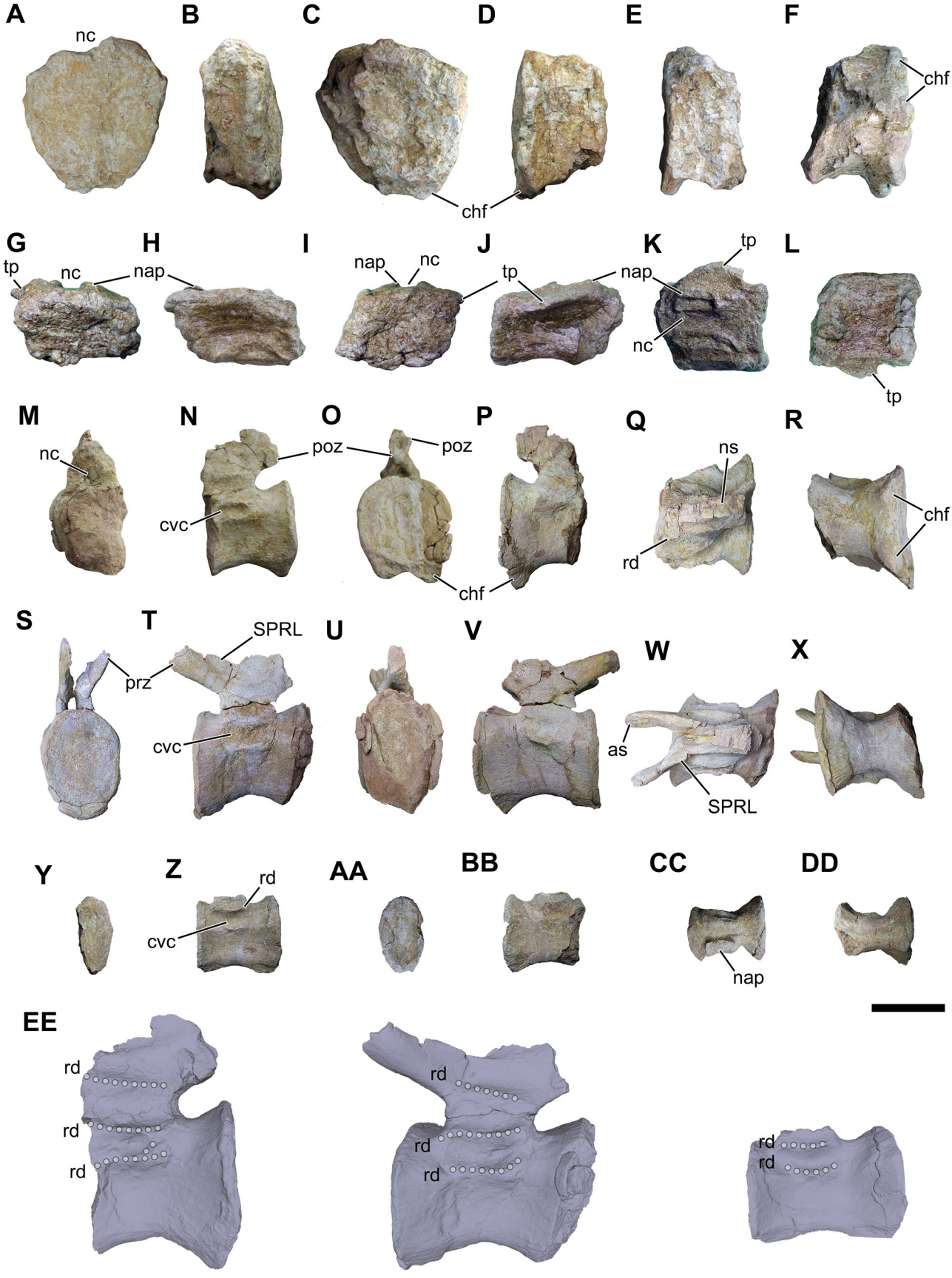
A
nc
B
C
chf
D
chf
E
F
chf
G
tp
nc
nap
H
I
nap
nc
J
tp
nap
K
tp
nc
L
tp
M
nc
N
poz
cvc
O
poz
chf
P
Q
ns
rd
R
chf
S
prz
T
SPRL
cvc
U
V
W
as
SPRL
X
Y
Z
rd
cvc
AA
BB
CC
nap
DD
EE
rd
rd
rd
rd
rd
rd
rd
rd

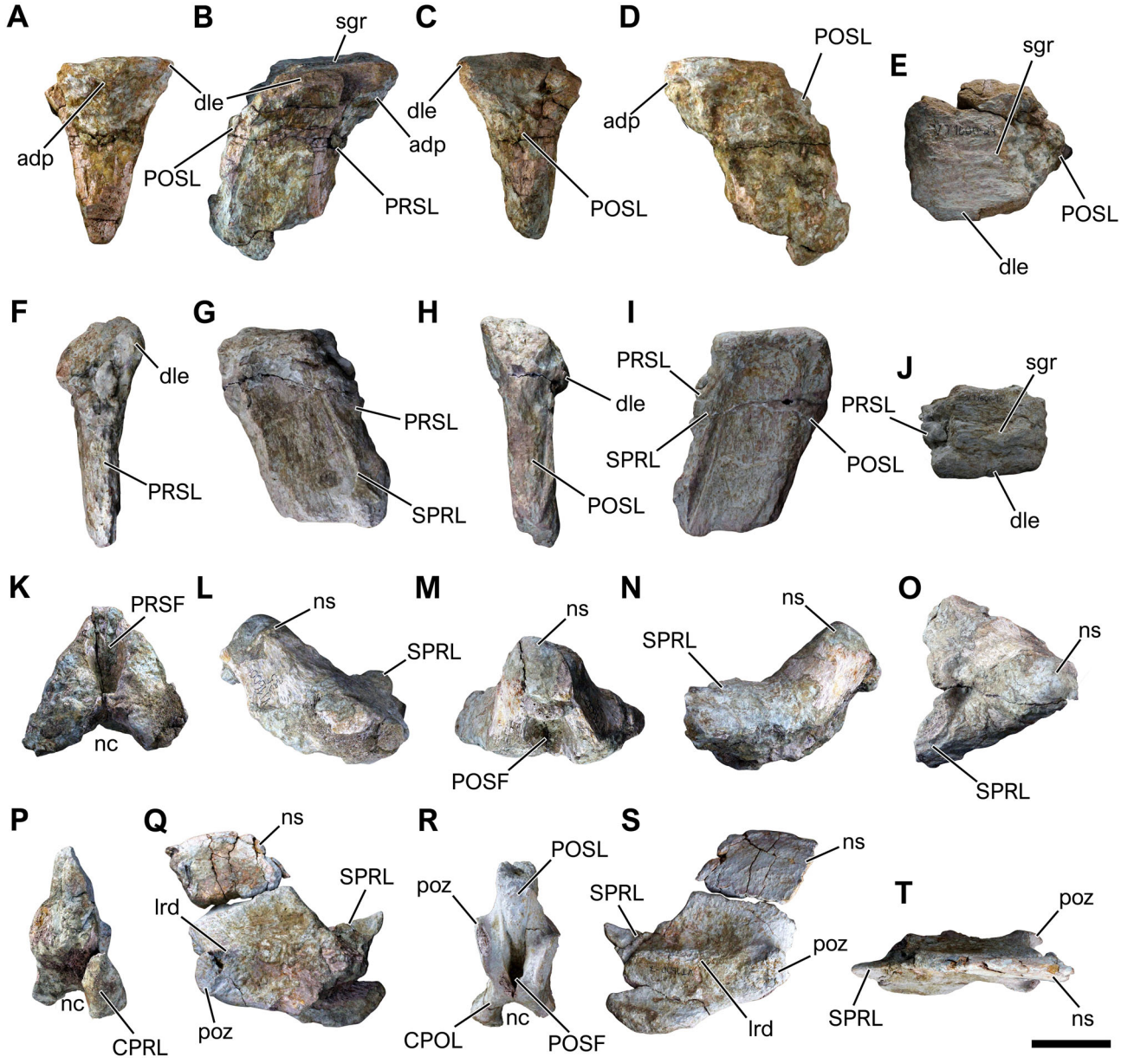

Figure 6. Additional caudal remains of *Dasosaurus tocantinensis* gen. et sp. nov. (CPHNAM VT 1600): **A–J,** isolated anterior caudal neural spines: **A–E,** CPHNAM VT 1600/11; **F–J,** CPHNAM VT 1600/12; **K–O,** partial anterior caudal neural arch (CPHNAM VT 1600/06); **P–T,** partial middle caudal neural arch (CPHNAM VT 1600/07); in anterior (A, F, K, P), right lateral (B, G, L, Q), posterior (C, H, M, R), left lateral (D, I, N, S), and dorsal (E, J, O, T) views. **Abbreviations**: **adp**, anterodorsal projection; **CPOL**, centropostzygapophyseal lamina; **CPRL**, centroprezygapophyseal lamina; **dle**, dorsolateral expansion; **lrd**, lateral ridge; **nc**, neural canal; **ns**, neural spine; **POSF**, postspinal fossa; **POSL**, postspinal lamina; **poz**, postzygapophysis; **PRSF**, prespinal fossa; **PRSL**, prespinal lamina; **sgr**, sagittal ridge; **SPRL**, spinoprezygapophyseal lamina. Scale bar = 5 cm.

Figure 5. Caudal vertebrae of *Dasosaurus tocantinensis* gen. et sp. nov. (CPHNAM VT 1600): **A–F,** more anteriorly placed anterior caudal centrum (CPHNAM VT 1600/1); **G–L,** more posteriorly placed anterior caudal centrum (CPHNAM VT 1600/2); **M–R,** middle caudal vertebra (CPHNAM VT 1600/3); **S–X,** middle to posterior caudal vertebra (CPHNAM VT 1600/4); **Y–DD,** posterior caudal centrum (CPHNAM VT 1600/5); **EE,** schematic models of the most complete caudal elements, indicating the three lateral ridges. Vertebrae in anterior (A, G, M, S, Y), left lateral (B, H, N, T, Z), posterior (C, I, O, U, AA), right lateral (D, J, P, V, BB), dorsal (E, K, Q, W, CC), and ventral (F, L, R, X, DD) views. **Abbreviations**: **as**, articular surface; **chf**, chevron facet; **cvc**, costovertebral concavity; **nap**, neural arch pedicel; **nc**, neural canal; **ns**, neural spine; **poz**, postzygapophysis; **prz**, prezygapophysis; **rd**, ridge; **SPRL**, spinoprezygapophyseal amina; **tp**, transverse process. Scale bar = 10 cm.

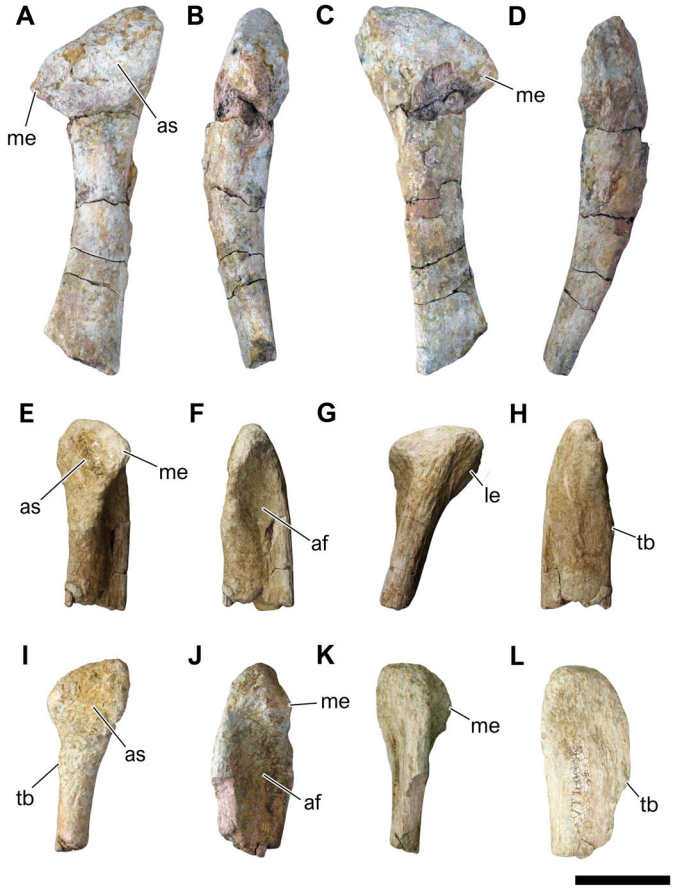

Figure 7. Chevron fragments of *Dasosaurus tocantinensis* gen. et sp. nov. (CPHNAM VT 1600/13): **A–D,** left haemal process of anterior chevron; **E–H,** right haemal process of anterior to middle chevron; **I–L,** left haemal process of posterior chevron. **Abbreviations**: **af**, anterior furrow; **as**, articular surface; **le**, lateral expansion; **me**, medial expansion; **tb**, tuberosity. Scale bar = 5 cm.

metacarpal II is ellipsoid, as in several other neosauropods (Apesteguía, 2005), with a convex lateral margin and a straight medial one. The articular surface has a rough texture and is slightly inclined anteroventrally in lateral view. As in most neosauropods, the shaft of metacarpal II is nearly straight in lateral/medial views, but subtly inclined anteromedially, differing from the more bowed condition seen in *L. leanzai* (Bonaparte et al., 2006) and from the trapezoidal distal outline of *C. insignis* (Apesteguía, 2005).

Metacarpal III preserves its proximal and distal ends, both of which have a rough texture. The articular surface is sub-triangular in proximal outline, with nearly straight margins, and slightly convex in lateral view due to a low proximal bowing. Its shaft has convex anterior and medial margins, whereas the posterior and lateral ones are slightly concave. In contrast, metacarpal III of *L. leanzai* is proportionally slenderer and bears a more robust posterior longitudinal crest (Bonaparte et al., 2006), whereas *C. insignis* has overall more robust metacarpals.

Metacarpal IV has a nearly trapezoidal distal outline, with a convex lateral margin. The medial margin is straight and rough proximally, accommodating the articulation for metacarpal V. In posterior view, a low intercondylar groove separates the rounded medial half of the distal surface from the more prominent lateral half, as also seen in *Venenosaurus dicrocei* (Tidwell et al., 2001) and *G. brancai* (Janensch, 1961). Unlike in *D. tocantinensis*, the metacarpals of *C. insignis* are slenderer and more elongate, with sub-rectangular distal outlines composed of more symmetrical medial and lateral condyles (Carballido et al., 2011). The metacarpals of *L. leanzai* are proximodistally shorter and more robust, with expanded distal ends and more evenly convex distal articular surfaces (Bonaparte et al., 2006), lacking the more pronounced intercondylar groove and lateral-medial disparity seen in *D. tocantinensis*.

Pelvic girdle and hind limb. Two portions of the left pubis were recovered: the iliac peduncle and the distal part of the shaft (CPHNAM VT 1600/19). The

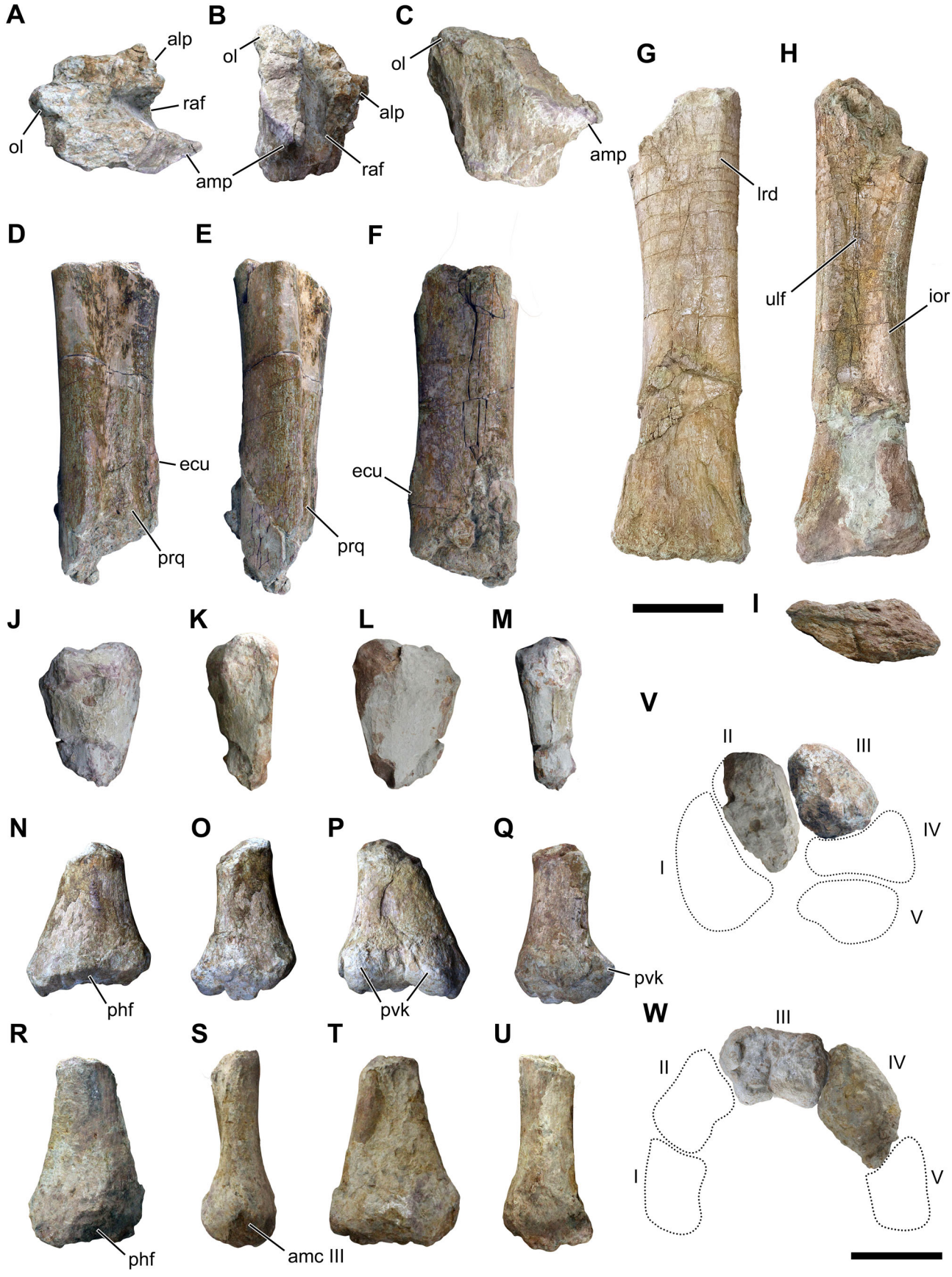
A
alp
raf
ol
amp
B
ol
alp
raf
C
ol
amp
G
lrd
H
ulf
ior
D
ecu
prq
E
prq
F
ecu
I
J
K
L
M
V
II
III
IV
I
V
N
phf
O
P
pvk
Q
pvk
W
III
II
IV
I
V
R
phf
S
amc III
T
U

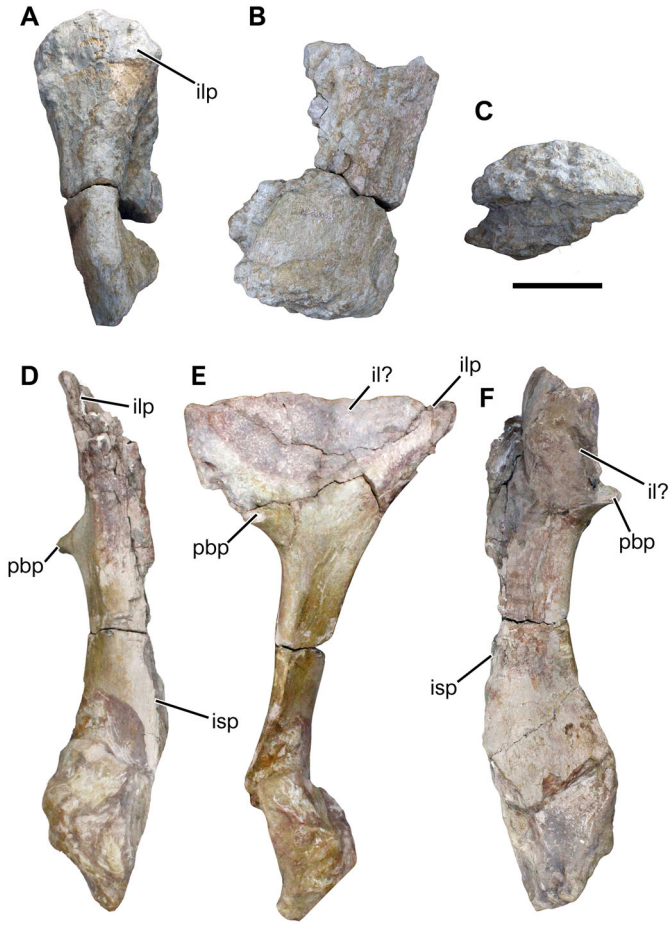

Figure 9. Pelvic girdle elements of *Dasosaurus tocantinensis* gen. et sp. nov. (CPHNAM VT 1600): **A,** proximal and **B, C,** distal ends of a left pubis (CPHNAM VT 1600/19) in **A,** anterior, **B,** lateral and **C,** distal views; **D–F,** partial left ischium (CPHNAM VT 1600/20) in **D,** posterior, **E,** posterolateral and **F,** anterior views. **Abbreviations**: **il**, ilium; **ilp**, iliac peduncle; **isp**, ischiadic process; **pbp**, pubic peduncle. Scale bar = 10 cm.

former expands lateromedially towards the proximal articulation with the ilium, which is mildly concave (Fig. 9A), as in *L. leanzai* (Bellardini et al., 2022, fig. 22B–G). Little of the apron was preserved, precluding an accurate identification of the pubic foramen. The preserved part of the shaft is transversely compressed. It expands anteroposteriorly towards the distal end, forming a somewhat sub-triangular lateral/medial outline (Fig. 9B). The distal end also expands lateromedially, so that the distal outline is flat medially and convex laterally (Fig. 9C). The distal surface is rugose and slight convex in lateral/medial views.

The partial left ischium (CPHNAM VT 1600/20) lacks part of the iliac peduncle and most of the ischiadic

Figure 8. Forelimb elements of *Dasosaurus tocantinensis* gen. et sp. nov. (CPHNAM VT 1600): **A–C,** proximal end of left ulna (CPHNAM VT 1600/15) in **A,** dorsal, **B,** medial and **C,** lateral views; **D–F,** distal half of left ulna (CPHNAM VT 1600/15) in **D,** medial, **E,** anterior, and **F,** lateral views; **G–I,** partial left radius (CPHNAM VT 1600/14) in **G,** lateral, **H,** medial and **I,** distal views; **J–M,** proximal end of right metacarpal II (CPHNAM VT 1600/16) in **J,** anterior, **K,** medial, **L,** posterior and **M,** lateral views; **N–Q,** distal end of right metacarpal III (CPHNAM VT 1600/17) in **N,** anterior, **O,** medial, **P,** posterior, and **Q,** lateral views; **R–U,** distal end of right metacarpal IV (CPHNAM VT 1600/18) in **R,** anterior **S,** medial, **T,** posterior and **U,** lateral views; right manus in **V,** proximal and **W,** distal views. Dotted lines represent non-preserved elements. Digit count shown in roman numerals. **Abbreviations**: **alp**, anterolateral process; **amc**, articulation with metacarpal; **amp**, anteromedial process; **ecu**, M. extensor carpi ulnaris insertion point; **ior**, interosseous ridge; **lrd**, lateral ridge; **ol**, olecranum process; **phf**, phalangeal facet; **prq**, M. pronator quadratus insertion point; **pvk**, posteroventrally projected knob; **raf**, radial fossa; **ulf**, ulnar fossa. Scale bars = 15 cm (A–I) and 10 cm (J–W).

process (Fig. 9D–F). The bone has an overall elongated shaft, as in *C. insignis* (Carballido et al., 2011, fig 13). The acetabular margin is slightly concave, although it is not well preserved. A plate-like bone is placed dorsal to the acetabular margin, creating a concave, anteroposteriorly broad surface, which probably corresponds to part of the ilium. The articulation with the pubis projects anteroventrally, as a narrow and elongated lip, unlike that of *Triunfosaurus leonardii* (Carvalho et al., 2017). The iliac peduncle projects dorsally with a rough articular surface, indicating firm contact with the ilium. The medial surface of the bone shows a short and thick symphysis, perpendicular to the long axis of the distal end of the shaft.

The preserved right femur (CPHNAM VT 1600/21; Fig. 10) lacks most of its distal end. In anterior/posterior views, the head is medially expanded and more proximally projected than the lateral corner of the proximal margin (i.e. the greater trochanter). The lateral-most portion of the femoral head is not as distally deflected as in *P. jonesi* and *T. sanzi* (Rose, 2007, fig. 27; Canudo et al., 2008, fig. 13), best resembling the morphology seen in *Ga. morellensis* (Mocho et al., 2022, fig. 12). Yet, the femur of *D. tocantinensis* is less eccentric (EI = 2.6) and robust (RI = 4.2) than that of the Spanish taxon (EI = 2.7–3.1; RI = 3.6–3.8; Mocho et al., 2023, table S4), although not as slender as that of *L. leanzai* (RI = 7.3). The shaft is anteroposteriorly compressed, with an elliptical cross-section *c*. 1.6 times broader lateromedially than anteroposteriorly and a concavity extending proximodistally along the proximal third of its posterior surface. The lateral bulge expands laterally from the proximal third of the bone (Fig. 10A, B), corresponding to 40% or more of its narrowest transverse width, as also seen in *Ga. morellensis*, *Neuquensaurus australis* and *Lirainosaurus astibiae* (Mocho et al., 2022; Salgado et al., 1997; Fig. 11). The fourth trochanter is placed posteromedially on the proximal half of the shaft, appearing as a thin ridge with a slight posterior inclination. It extends beyond the distal margin of the lateral bulge, differing from the condition in *Ga. morellensis* (Mocho et al., 2023), the trochanter of which is aligned with the distal margin of that bulge. The anterior surface of the femur lacks a linea intermuscularis cranialis, as seen in *Ga. morellensis* (Mocho et al., 2023). Due to poor preservation on the posterior surface, the presence of a trochanteric shelf, as seen in this later taxon, could not be assessed.

The preserved proximal half of a left tibia (CPHNAM VT 1600/22; Fig. 10C–G) reveals a highly anteroposteriorly expanded proximal end. Its proximal outline is ovoid, as in some specimens of *Ga. morellensis* (Mocho et al., 2023, fig. 14I), but not as lateromedially compressed as in *S. proteles* and *P. jonesi* (D'Emic, 2012, fig. 3.14; Rose, 2007, fig. 28). It is also not subsquared, as in the paratypic specimen of *Ga. morellensis* (Mocho et al., 2023, fig. 14), as well as in *Lusotitan atalaiensis* (Mannion et al., 2013, fig. 17) and *T. sanzi* (Canudo et al., 2008, fig. 14). In proximal view, the cnemial crest projects anterolaterally and is laterally bound by a narrow cnemial fossa. Lateral to that, a bulge expands slightly distally along the lateral surface for the articulation for the fibula. Its proximal surface bears a subtle anterior projection, which seems to correspond to an accessory cnemial crest (the 'second cnemial crest' of Bonaparte et al., 2000). As in *Ga. morellensis*, a posteromedial prominence is present, but more developed than in that species. In lateral/medial views, the cnemial crest is sub-triangular, with a pointed tip like that of *T. sanzi*, as opposed to the rounded contours seen in most other somphospondyls (Canudo et al., 2008, fig. 14). The tibia has a relatively slender shaft, with a strongly lateromedially compressed proximal end, as in *C. insignis* (Carballido et al., 2011), but with a more anteroposteriorly expanded and prominent cnemial crest. The tibia of *L. leanzai* is more robust and proportionally shorter than that of the new species (Bellardini et al., 2022), with a mediolaterally broader proximal outline and a mainly anteriorly, rather than anterolaterally projecting cnemial crest. The shaft has a sub-circular cross-section at its preserved distal end, with the medial surface presenting a proximodistally elongated groove. The bone bears a poorly preserved lateral trochanter, expanding from its posterolateral surface.

Preserved fibular portions include the proximal end of the left element (CPHNAM VT 1600/23; Fig. 10H–L) and the distal half of the right one (CPHNAM VT1600/24; Fig. 10M–P). The bone is more compressed than that of *Ga. morellensis*, but mainly straight as in the Spanish taxon, lacking the pronounced sigmoid shape seen in late diverging somphospondyls. As preserved, the proximal outline of the fibula is elliptical, with an anteroposterior long axis. A prominent, sub-triangular tuberosity is present laterally on the proximal surface but detached from the lateral trochanter (Fig. 10I, J). Unfortunately, the incompleteness of the specimen prevents the identification of the crest close to the lateral trochanter seen in *Ga. morellensis* (Mocho et al., 2023, fig. 15). Additionally, its anterior and posterior margins respectively bear a scar for M. popliteus and the insertion point of M. flexor digitorum longus (Voegele et al., 2020). As in *Ga. morellensis*, the preserved portion of the shaft is nearly straight anteriorly and slightly convex posteriorly. The tibial articulation is concave and delimited by an interosseous ridge, whereas the distal portion

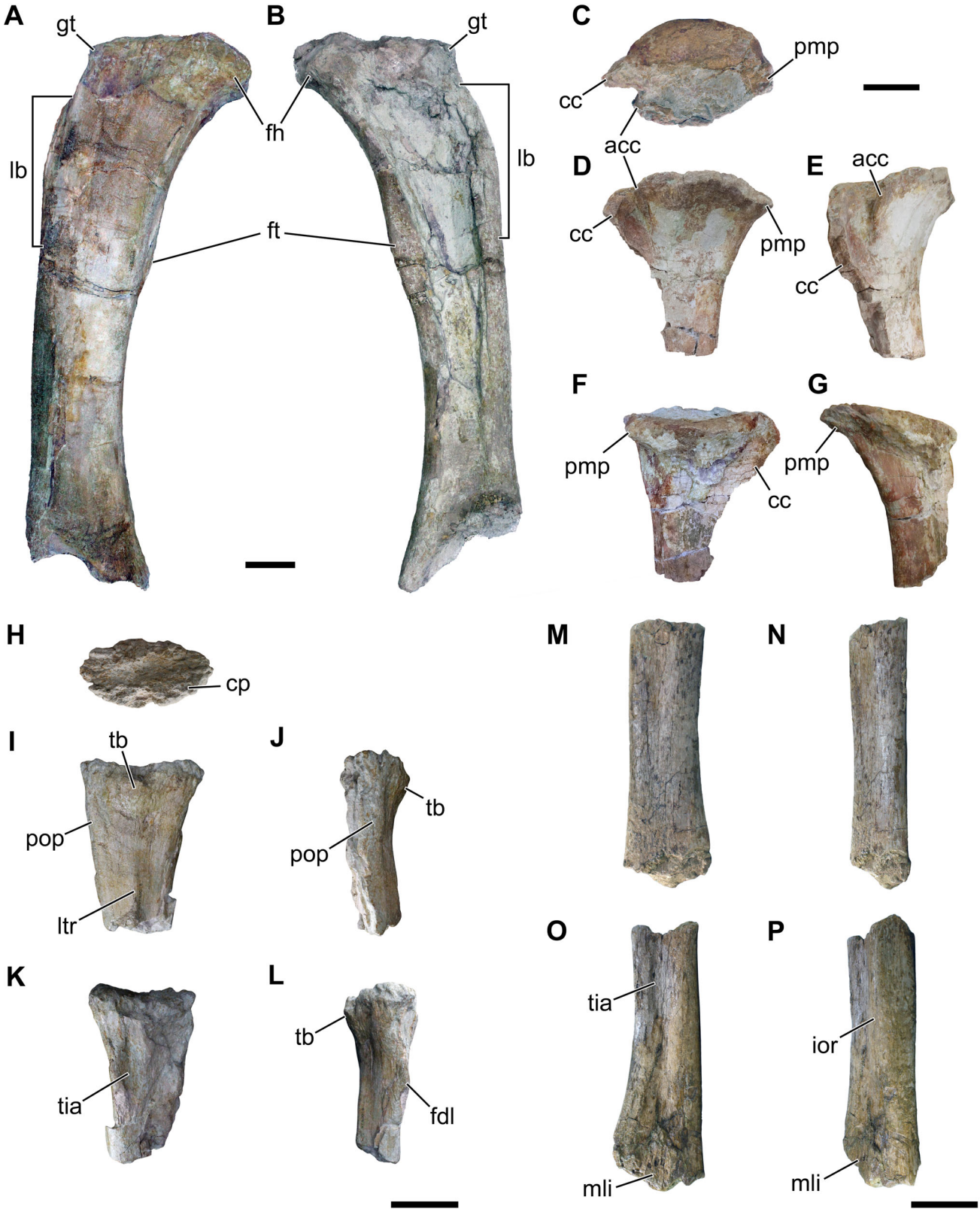
A
gt
lb
fh
ft
B
gt
lb
C
pmp
cc
acc
D
cc
pmp
E
acc
cc
F
pmp
cc
G
pmp
H
cp
I
tb
pop
ltr
J
tb
pop
K
tia
L
tb
fdl
M
N
O
tia
mli
P
ior
mli

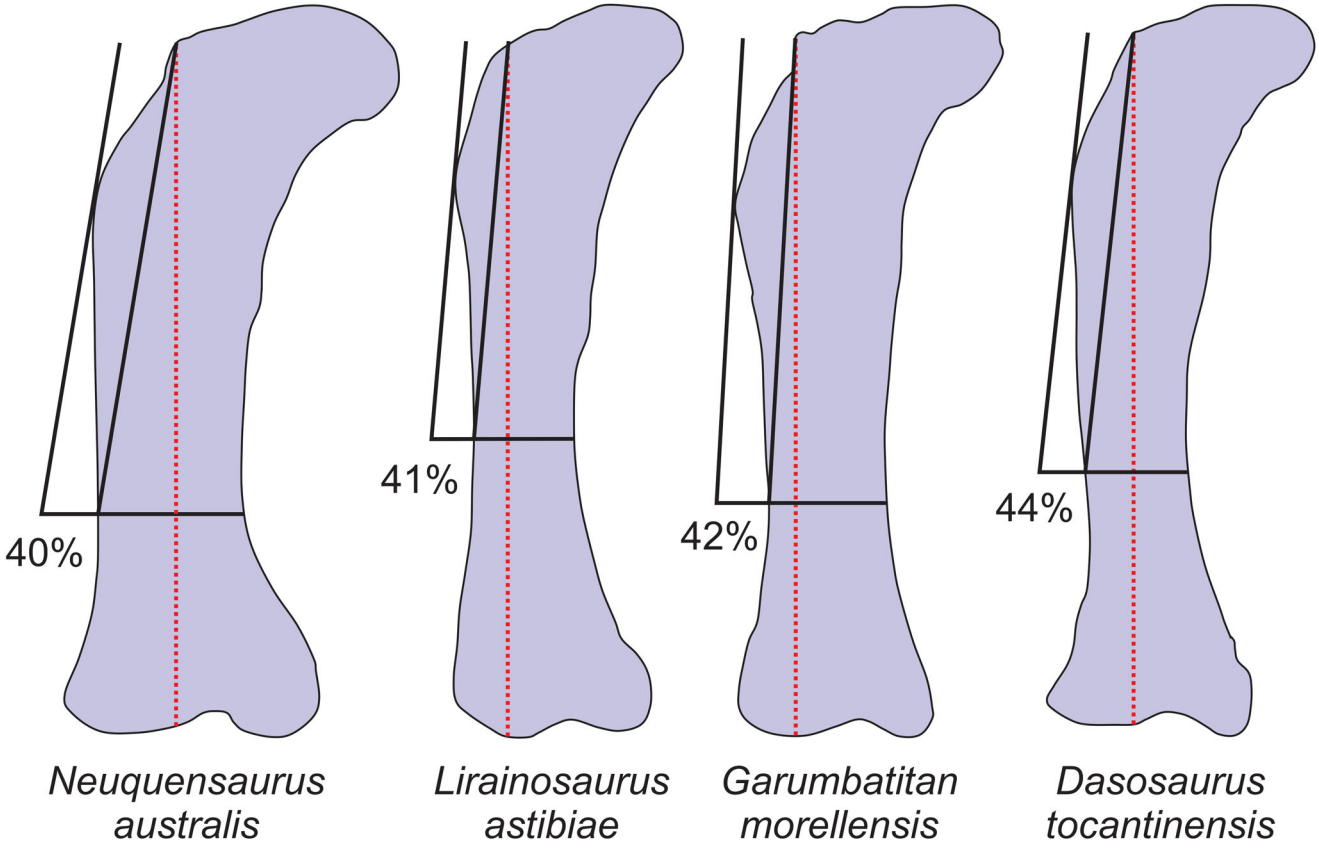

Figure 11. Anterior/posterior outlines of selected titanosauriform femora (not at the same scale), in which the lateral bulge corresponds to 40% or more of the minimal transverse width of the shaft (after Mannion et al., 2013; Mocho et al., 2022; Salgado et al., 1997).

is marked by the presence of a medial lip for the calcaneal articulation. In *C. insignis*, the fibula is also straight, but proportionally more gracile, with a less prominent lateral tuberosity (Carballido et al., 2011), whereas it is relatively stouter in *L. leanzai*, with a subrectangular proximal outline (Bellardini et al., 2022), both differing from the morphology seen in the new species.

The pedal elements (Fig. 12) were identified based upon comparisons with an array of complete, articulated pedes, including those of *Epachthosaurus sciuttoi* (Martínez et al., 2004), *Gobititan shenzhouensis* (You et al., 2003), the 'La Invernada' titanosaur (González Riga et al., 2008), and *Ga. morellensis* (Mocho et al., 2023), allowing their assignment to a left pes with a possible 2-3-3-2?-2? phalangeal formula. Metatarsal II (CPHNAM VT 1600/25; Fig. 12A–F) has a lateromedially expanded proximal end, whereas the shaft is slender, with concave lateral and medial margins. Both proximal and distal ends are deflected in respect to the long axis of the shaft: the proximal one turns medially and the distal one laterally. The ventral surface has a rounded ridge extending distally from the medial portion of the proximal articulation. This medially borders a concave area where metatarsal III would articulate. Its distal end, as well as that of metatarsal III (CPHNAM

Figure 10. Hind limb elements of *Dasosaurus tocantinensis* gen. et sp. nov. (CPHNAM VT 1600): **A, B,** right femur (CPHNAM VT 1600/21) in **A,** anterior and **B,** posterior views; **C–G,** proximal end of left tibia (CPHNAM VT 1600/22) in **C,** proximal, **D,** lateral, **E,** anterior, **F,** medial and **G,** posterior views; **H–L,** proximal end of left fibula (CPHNAM VT 1600/23) in **H,** proximal, **I,** lateral, **J,** anterior, **K,** medial and **L,** posterior views; **M–P,** distal half of right fibula (CPHNAM VT 1600/24) in **M,** lateral, **N,** anterior, **O,** medial and **P,** posterior views. **Abbreviations**: **acc**, accessory cnemial crest; **cc**, cnemial crest; **cp**, cartilage pits; **fdl**, M. flexor digitorum longus insertion point; **fh**, femoral head; **ft**, fourth trochanter; **gt**, greater trochanter; **ior**, interosseous ridge; **lb**, lateral bulge; **ltr**, lateral trochanter ridge; **mli**, medial lip; **pmp**, posteromedial prominence; **pop**, M. popliteus insertion point; **tb**, tuberosity; **tia**, tibial articular surface. Scale bars = 15 cm (A–G) and 10 cm (H–P).

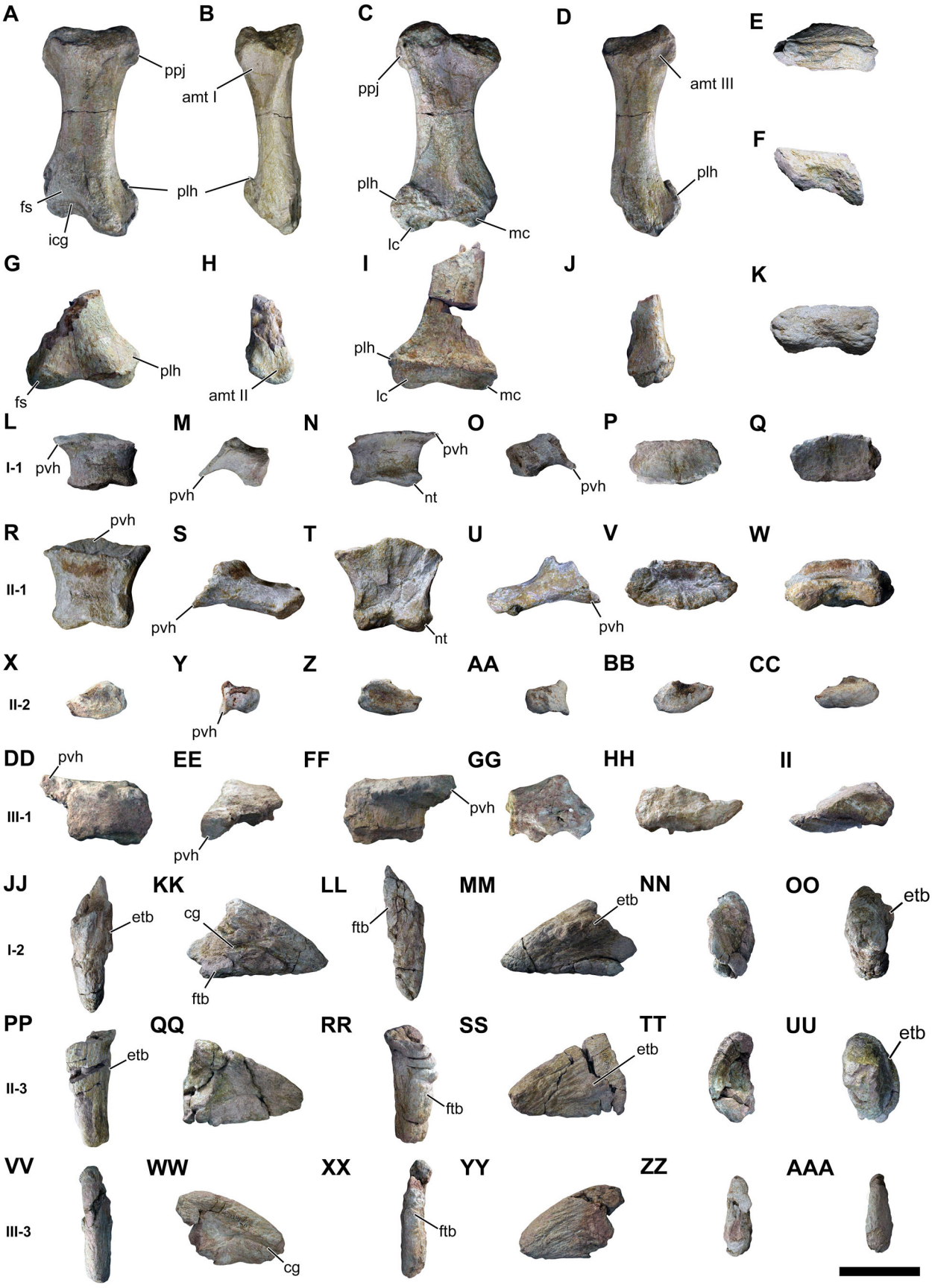
A
ppj
fs
icg
plh
B
amt I
plh
C
ppj
plh
lc
mc
D
amt III
plh
E
F
G
plh
fs
H
amt II
I
plh
lc
mc
J
K
L
I-1
pvh
M
pvh
N
pvh
nt
O
pvh
P
Q
R
II-1
pvh
S
pvh
T
nt
U
pvh
V
W
X
II-2
Y
pvh
Z
AA
BB
CC
DD
III-1
pvh
EE
pvh
FF
GG
pvh
HH
II
JJ
I-2
etb
KK
cg
ftb
LL
ftb
MM
etb
NN
OO
etb
PP
II-3
etb
QQ
RR
ftb
SS
etb
TT
UU
etb
VV
III-3
WW
cg
XX
ftb
YY
ZZ
AAA

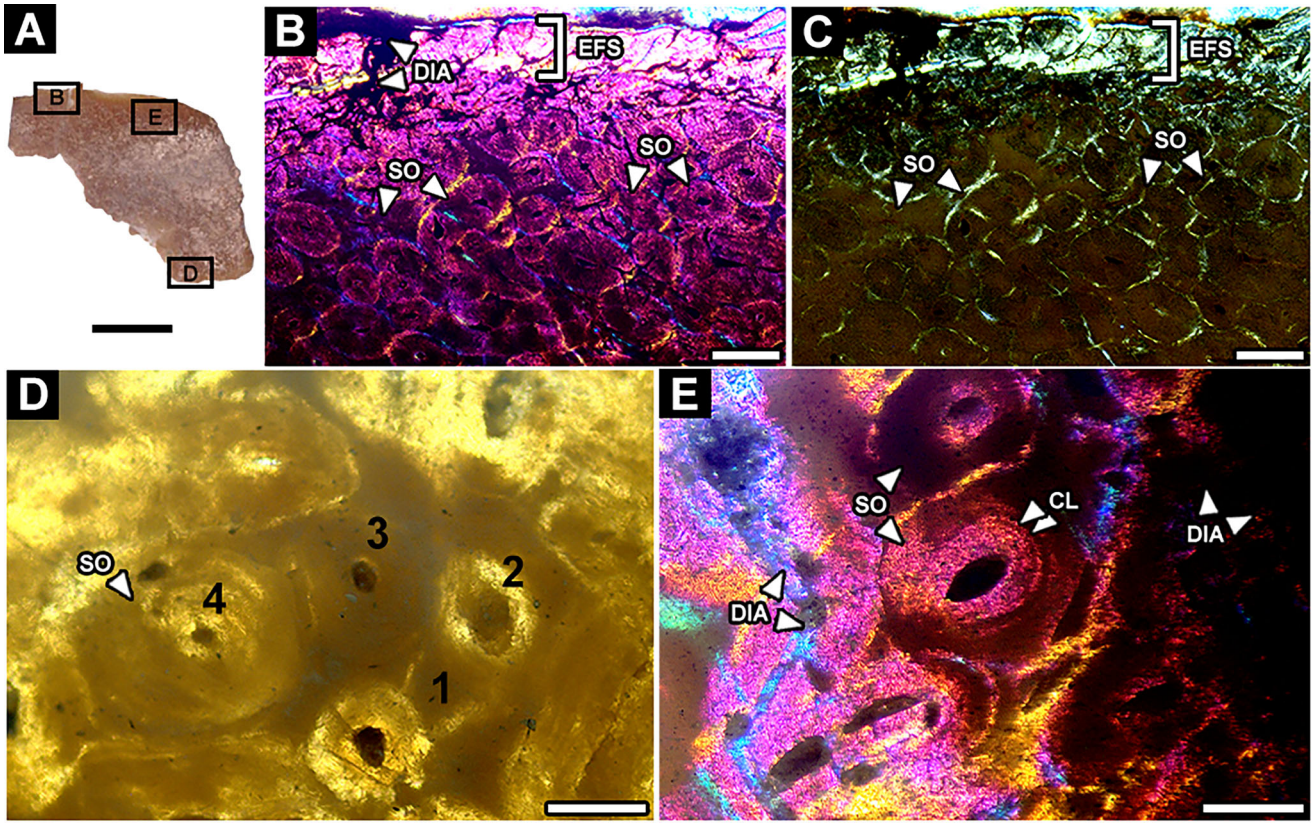

Figure 13. Femur histology of *Dasosaurus tocantinensis* gen. et sp. nov. (CPHNAM VT 1600/34). **A,** midshaft cross-section of the medial portion showing areas detailed in B–E; **B, C,** EFS in the subperiosteal surface; **D, E,** extensive secondary remodelling on the outer cortex, with at least three generations of secondary osteons (**D**), each containing several centripetal layers (**E**). Normal transmitted (A) and polarized light with parallel (D) and crossed nicols with (B, E) and without (C) lambda compensator. **Abbreviations**: **DIA**, diagenetic artefacts; **EFS**, external fundamental system; **SO**, secondary osteons. Scale bars = 10 mm (A), 200 μm (B, C) and 100 μm (D, E).

VT-1600/26; Fig. 12G–K), is also lateromedially expanded, forming the ginglymoid facet, which is more strongly concave between the condyles in CPHNAM VT 1600/25 than in CPHNAM VT-1600/26. The medial and lateral condyles are composed of two small posteriorly projecting knobs, differing from the nearly flat distal surface present in *L. leanzai* (Bellardini et al., 2022, fig. 26).

All preserved phalanges were identified as pedal elements, i.e. I-1 (CPHNAM VT 1600/27; Fig. 12L–Q), II-1 (CPHNAM VT 1600/28; Fig. 12R–W), II-2 (CPHNAM VT 1600/29; Fig. 12X–CC), and III-1 (CPHNAM VT 1600/30; Fig. 12DD–II), as well as ungual phalanges I–III (CPHNAM VT 1600/31–33; Fig. 12JJ–AAA). They have slightly concave proximal and convex distal surfaces and sub-rectangular outlines in dorsal/plantar views, with concave lateral and medial margins. In the plantar surface, both non-ungual phalanges have a strong medial projection of the proximoventral margins (Fig. 12), more accentuated than those observed in *Ga. morellensis* (Mocho et al., 2023, fig. 20). As also seen in the metatarsals, the distal end of the non-ungual phalanges are lateromedially expanded, forming the ginglymoid facets that are strongly concave

Figure 12. Left pes of *Dasosaurus tocantinensis* gen. et sp. nov. (CPHNAM VT 1600): **A–F,** metatarsal II (CPHNAM VT 1600/25); **G–K,** partial metatarsal III (CPHNAM VT 1600/26); **L–Q,** pedal phalanx I-1 (CPHNAM VT 1600/27); **R–W,** pedal phalanx II-1 (CPHNAM VT 1600/28); **X–CC,** pedal phalanx II-2 (CPHNAM VT 1600/29); **DD–II,** pedal phalanx III-1 (CPHNAM VT 1600/30); **JJ–OO,** ungual I (CPHNAM VT 1600/31); **PP–UU,** ungual II (CPHNAM VT 1600/32); **VV–AAA,** ungual III (CPHNAM VT 1600/33). From left to right: dorsal, medial, ventral, lateral, proximal, and distal views. **Abbreviations**: **amt**, articulation with metatarsal; **cg**, collateral groove; **etb**, extensor tubercle; **fs**, flexor surface; **ftb**, flexor tubercle; **icg**, intercondylar groove; **lc**, lateral condyle; **mc**, medial condyle; **nt**, notch; **plh**, posterolateral hook; **ppj**, proximal projection; **pvh**, posteroventral heel. Scale bar = 10 cm.

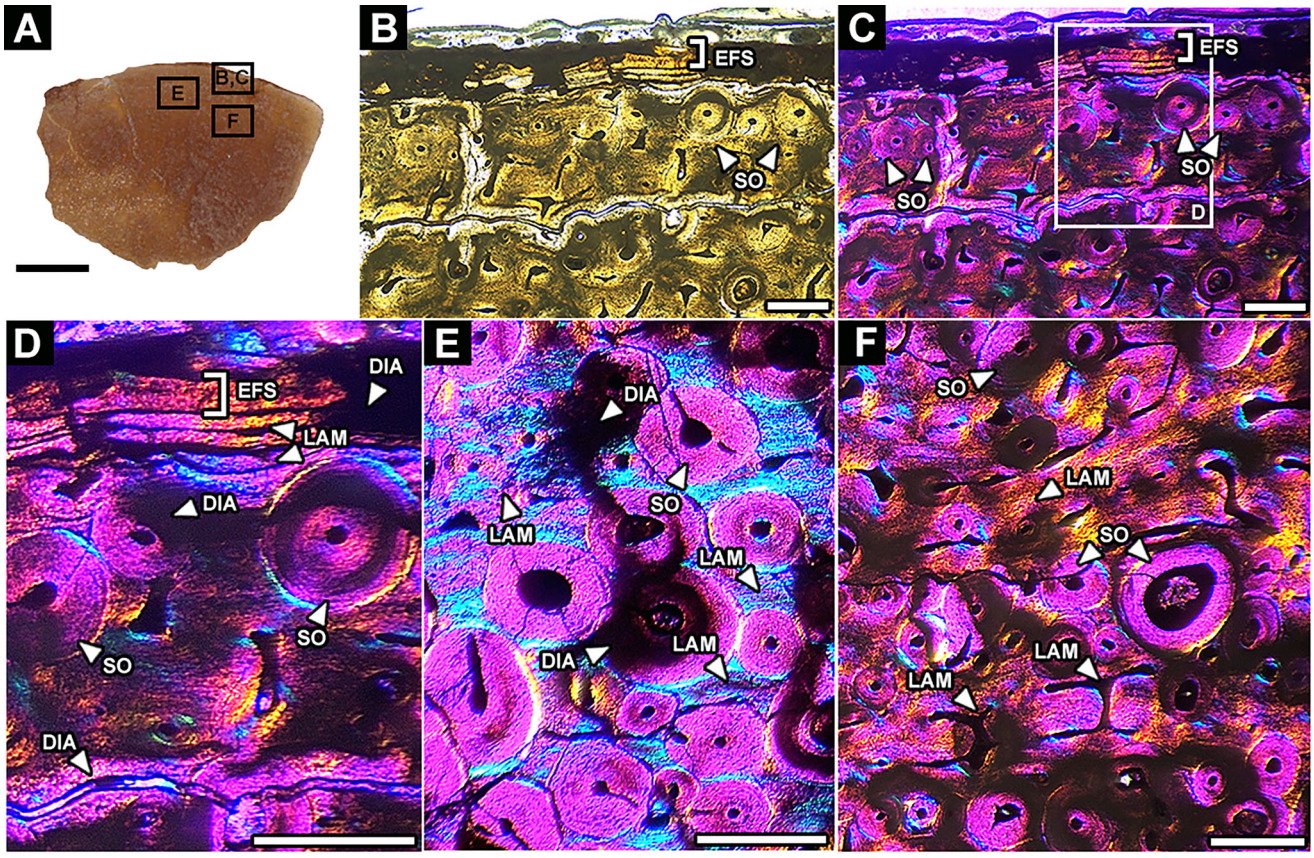

Figure 14. Tibia histology of *Dasosaurus tocantinensis* gen. et sp. nov. (CPHNAM VT 1600/34). **A,** midshaft cross-section showing the areas detailed in **B**–**F**; **B**–**D,** photomicrographs showing an EFS in the periosteum; **E, F,** secondary osteons over the remaining primary tissue, including laminar vascularization. Normal transmitted (A) and polarized light with parallel (B) and crossed nicols with lambda compensator (C–F). **Abbreviations**: **DIA**, diagenetic artefacts; **EFS**, external fundamental system; **LAM**, laminar vascularization; **SO**, secondary osteons. Scale bars = 10 mm (A), 200 μm (B–F).

between the condyles, particularly in II-1 and III-1, where second phalanges (II-2 and III-2) articulate.

The ungual phalanges are robust and sickle-shaped. Their plantar surfaces are broader than in *Ga. morellensis*, so that the proximal outlines are sub-triangular to elliptical. The first and second ungual phalanges are subequal in length, whereas the third is about two-thirds of their lengths. Their external surfaces are heavily sculptured, whereas the lateral grooves are incipient. All ungual phalanges bear a marked tuberosity in their dorsolateral surface, which extends ventrally along the lateroventral side of the bone. These are interpreted here as extensor tubercles, representing a putative autapomorphy of *D. tocantinensis*. The flexor tubercles are robust, especially at their lateral portions, and occupy most of the proximal portion of the ventral surface of the bones.

Osteohistology

The histology of the femur shows intense secondary remodelling (Fig. 13B, C), with at least three generations of Harversian osteons (Fig. 13D), each containing three or more centripetal layers (Fig. 13E). In the outer cortex, LAGs are completely obscured by remodelling, a condition common among somphospondyls, especially titanosaurs (see discussion below). Nevertheless, the subperiosteal surface exhibits the characteristic organization of an external fundamental system (EFS): a thick, avascular superficial layer with anomalous birefringence when compared with the outer cortex (Fig. 13B, C). The histology of the tibia (Fig. 14) also preserves an EFS (Fig. 14B–D) and shows intense secondary remodelling (Fig. 14B–F). Unlike the femur microstructure, primary tissue is still preserved in some areas (laminar vascularization; Fig. 14E, F), comprising laminar vascularization with sparse primary osteons. In these areas, osteocyte lacunae seem disorganized in contrast of the centripetal pattern seen in the Harversian osteons. Only two generations of Harversian osteons are preserved, with up to five centripetal layers. The thin section of the rib (Fig. 15) shows no EFS and a considerable amount of subperiosteal lamellar tissue containing

abundant Sharpey's fibres in the outer cortex (Fig. 15B–D). The cortex shows intense secondary remodelling (Fig. 15E). There is no pyrophosphate biomineralization over the subperiosteal surface of the femur, tibia, or rib. The intense secondary remodelling in the femur and tibia, plus the presence of EFS on both suggests that the individual was an adult at time of death (Francillon-Viellot et al., 1990). The several generations of secondary osteons and many circumferential centripetal layers on each osteon suggest a mature ontogenetic status, but the absence of pyrophosphate biomineralization discards a senile condition (Słowiak et al., 2021).

Phylogenetic and biogeographic results

The equal weights analysis found 232 MPTs of 2.713 steps (source data file 7 available through OSF; Godoy, 2025). It is worth mentioning that, given the nature of the search protocol, the number of MPTs can vary depending on the iteration. For this analysis, we expect the number of obtained MPTs to vary between 200 and 300. The consensus of the 232 MPTs (see Supplemental material) shows a polytomy around Titanosauriformes, including *Europasaurus holgeri*, *Galvesaurus herreroi*, brachiosaurids and somphospondyls. The latter group is also composed of a polytomy, including the *Ga. morellensis* plus *D. tocantinensis* clade, among many other taxa and clades, the larger of which broadly corresponds to Titanosauria.

The implied weighting analysis yielded 59 MPTs of '141.21333' steps (see source data file 8, available through OSF; Godoy, 2025). Again, the number of MPTs can vary depending on the iteration, but we expect a number between 50 and 70. The consensus (Fig. 16; Supplemental material) is better resolved in comparison to the equal weights analysis, showing *Huanghetitan liujiaxiaensis* as the earliest-branching somphospondyl, instead of *Dongbeititan dongi* as in Mocho et al. (2023). Also, unlike Mocho et al. (2023), the next clade does not include a dichotomy between *Ga. morellensis* and the bulk of somphospondyls, but a polytomy with *Angolatitan adamastor*, *Do. dongi*, *Wintonotitan wattsi*, and two clades, one formed by *Padillasaurus leivaensis* plus *C. insignis*, and another by the other somphospondyls. This latter includes four successive branches, i.e. a polytomy with *P. jonesi*, *S. proteles*, and the 'Clovery titanosauriform' (1), *L. leanzai* (2), the clade with *Ga. morellensis* and *D. tocantinensis* (3), and *T. sanzi* plus *Europatitan eastwoodi* (4), as sister to a large monophylum including Euhelopodidae plus Titanosauria. The euhelopodid lineage includes not only all Euhelopodidae of Mocho et al. (2023) but also forms placed by those authors in a clade outside of

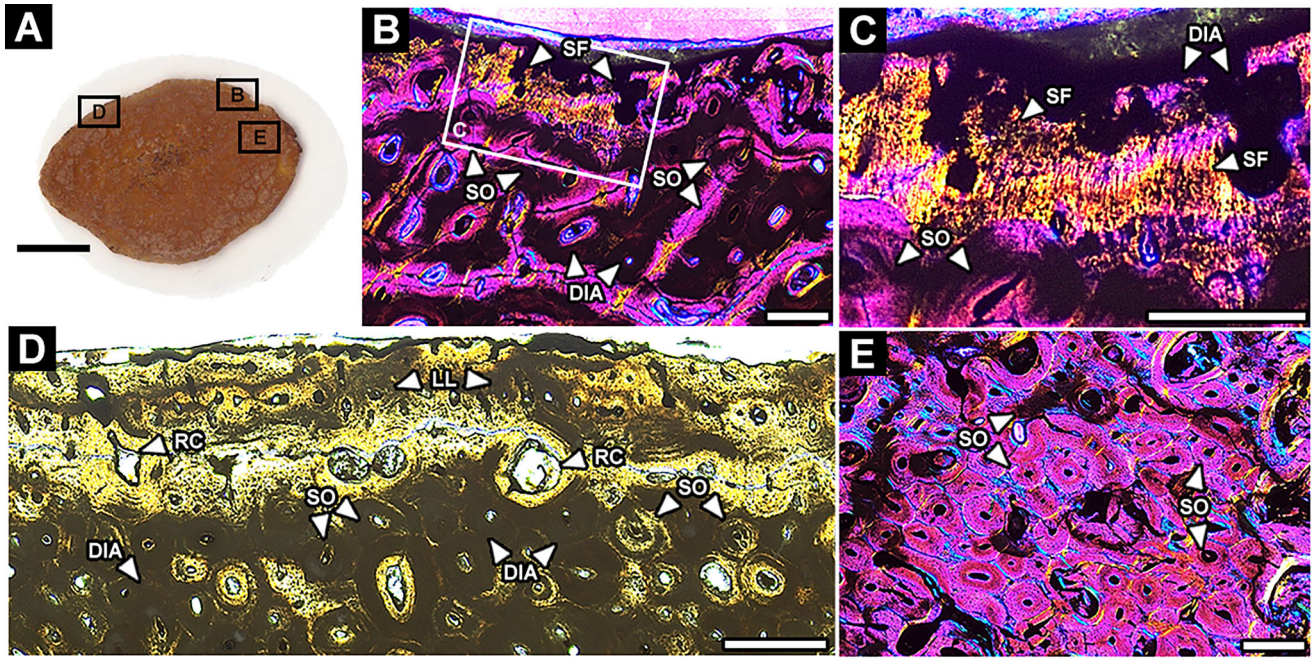

Figure 15. Rib histology of *Dasosaurus tocantinensis* gen. et sp. nov. (CPHNAM VT 1600/34). **A,** cross-section showing the areas detailed in B–E; **B, C,** photomicrographs showing Sharpey's fibres in the periosteum; **D,** secondary remodelling up to the outer cortex, where a short layer of primary lamellar bone remains in association with resorption cavities; **E,** inner and middle cortex areas completely populated by secondary osteons. Normal transmitted (A) and polarized light with parallel (D), and crossed (B, C, E) nicols with lambda compensator. **Abbreviations**: **DIA**, diagenetic artefacts; **EFS**, external fundamental system; **LL**, primary lamellar bone; **RC**, resorption cavity; **SF**, Sharpey's fibres; **SO**, secondary osteons. Scale bars in = 10 mm (A), 200 μm (B–E).

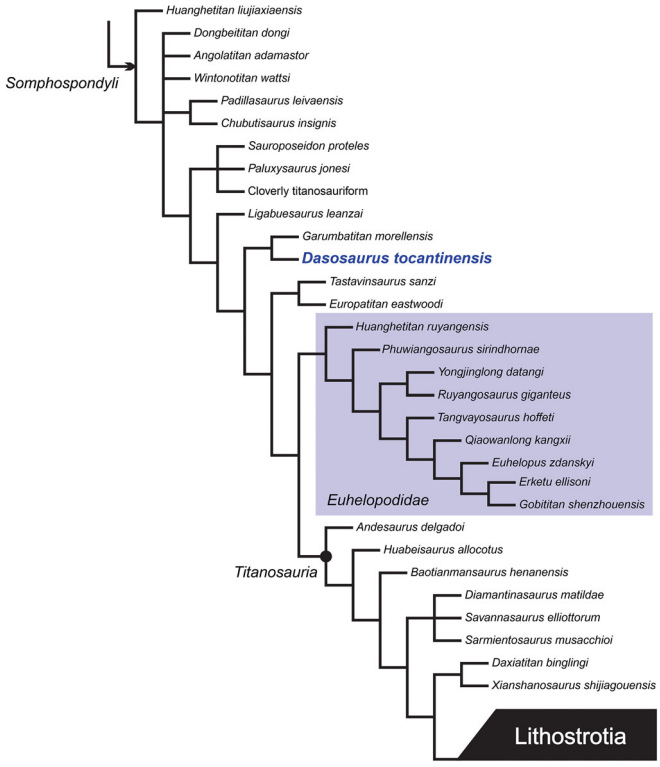

Figure 16. Phylogenetic hypothesis showing the position of *Dasosaurus tocantinensis* gen. et sp. nov. as a non-titanosaur Somphospondyli. Abridged version of the consensus tree found in the implied weighting analysis.

Euhelopodidae plus Titanosauria (i.e. *G. shenzhouensis*, *Erketu ellisoni* and *H. ruyangensis*).

The dispersal and extinction rates, as well as the maximum likelihoods for each DEC analysis, can be found in the ancestral state reconstruction plots (see Supplemental material and source data file 9, available through OSF; Godoy, 2025). All 10 time-calibrated trees indicate an origin for Somphospondyli around the Jurassic-Cretaceous boundary – four during the latest Jurassic, five crossing the boundary, and one at the earliest Cretaceous – and a broad ancestral range (Fig. 17), including Europe (all trees), Asia (all trees), southern South America (nine trees), as well as Laramidia (four trees) and Appalachia (one tree). Within that group, the divergence time of the lineage including *Ga. morellensis* and *D. tocantinensis* was also set around the Jurassic–Cretaceous boundary, but with a strong trend (eight trees) towards the earliest Cretaceous. All analysed trees also indicate a broad ancestral range, including Europe, Asia and southern South America, for the clade including the *Ga. morellensis* plus *D. tocantinensis* lineage and its sister group (Fig. 17). As for the *D. tocantinensis* plus *Ga. morellensis* dichotomy, its age is set between the Valanginian and Aptian in nine of the 10 analysed trees; the outlier corresponding to a Tithonian range. Area reconstructions for all trees point to a European origin (Fig. 17).

Further along Somphospondyli, the divergence time of the clade including Euhelopodidae plus Titanosauria was also set either at the earliest Cretaceous (seven trees) or crossing the Jurassic–Cretaceous boundary (three trees). An ancestral range including only Asia and southern South America (Fig. 17) was reconstructed for the clade in nine of the 10 analysed trees (one tree also including Europe), with Euhelopodidae showing an evolutionary history restricted to Asia. As for Titanosauria, its ancestral range was reconstructed as southern South America and Asia in all analysed trees (Fig. 17), also including southern Africa in three of those, along with Europe in one and Indo-Madagascar in another. As for its time of origin (see also Gorscak & O'Connor, 2016), nine of the trees point towards an Early Cretaceous (Berriasian-Aptian) range, with a Tithonian-Berriasian outlier. Within Titanosauria, a Valanginian-Aptian origin was inferred for Lithostrotia. Indeed, its ancestral range was reconstructed to southern South America and southern Africa in all analysed trees, with Indo-Madagascar added in two of them, but Asia was also included in all trees and Europe in half of them (Fig. 17).

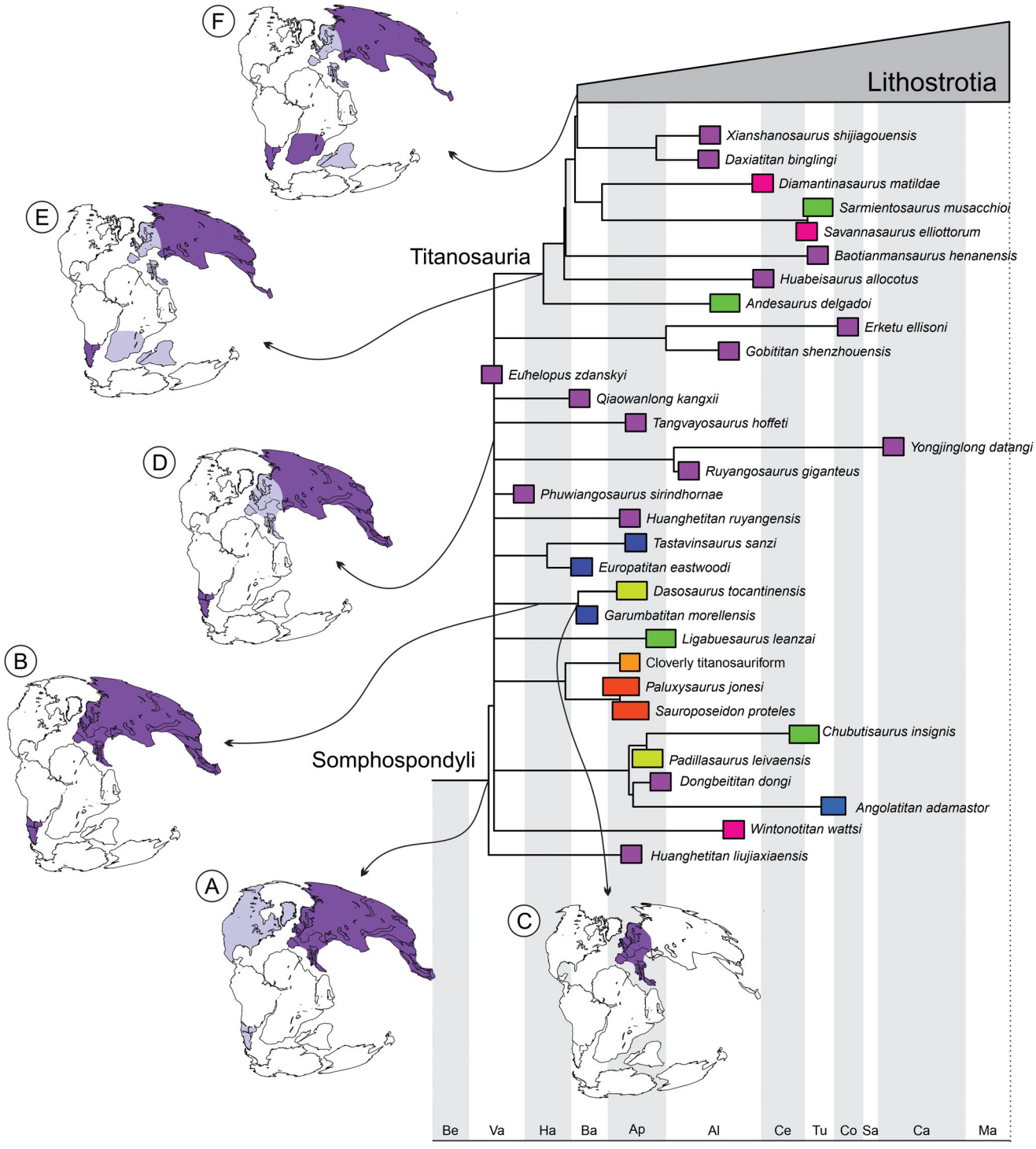

Figure 17. Time-calibrated tree no. 9. Colour scheme: Appalachia (red), Asia (purple), Australasia (pink), Europe (dark blue), Laramidia (orange), southern Africa (light blue), northern South America (yellow), and southern South America (green). Maps showing ancestral areas (coloured) for selected clades: **A,** Somphospondyli; **B,** *Ga. morellensis* + *D. tocantinensis* plus its sister-clade; **C,** *Ga. morellensis* + *D. tocantinensis*; **D,** Titanosauria + Euhelopodidae; **E,** Titanosauria; **F,** Lithostrotia. 140–125 (A, C, D) and 125–120 (B, E, F) myrs maps from Upchurch and Chiarenza (2024). Dark purple = ancestral areas reconstructed in all trees, light purple = ancestral areas reconstructed only in some trees. **Abbreviations**: **Al**, Albian; **Ap**, Aptian; **Ba**, Barremian; **Be**, Berriasian; **Ca**, Campanian; **Ce**, Cenomanian; **Co**, Coniacian; **Ha**, Hauterivian; **Ma**, Maastrichtian; **Sa**, Santonian; **Tu**, Turonian; **Va**, Valanginian.

Discussion

Osteohistology

Titanosauriforms bear the most metabolic-demanding growth rates of all sauropods (Curry-Rogers & Kulik, 2018; Mitchell & Sander, 2014; Navarro et al., 2022; Sander et al., 2006). A large *G. brancai* adult has extensive secondary remodelling, but still shows most of the primary vascularization, also seen in earlier neosauropods and diplodocoids (Hedrick, 2012; Klein & Sander, 2008; Mitchell & Sander, 2014; Windholz & Cerda, 2021). Conversely, the histological profile of adult titanosaurs shows very high rates of secondary remodelling, completely obliterating the early life histological record, as seen in taxa such as *Alamosaurus sanjuanensis*, *Ampelosaurus atacis*, *Ibirania parva*, *Magyarosaurus dacus*, and *R. krausei* (Curry-Rogers & Kulik, 2018; Klein et al., 2012; Navarro et al., 2022; Stein et al., 2010; Woodward, 2005). This succession of secondary remodelling is intense enough to obliterate even the EFS of most taxa (Curry-Rogers & Kulik, 2018; Navarro et al., 2022; Stein et al., 2010).

Most sampled titanosauriforms belong to either the phylogenetically disparate Brachiosauridae or Titanosauria. Histological data on non-brachiosaurid and non-titanosaur titanosauriforms is scarce, and such data-gaps hamper the depiction of where phylogenetically, the shift towards a higher metabolic rate occurred. The histology pattern of *D. tocantinensis* is intermediate between that of early neosauropods and titanosaurs. It preserved the EFS and portions of primary tissue as in the former group, as well as a high degree of secondary osteons, as in the latter clade. Indeed, the adult *D. tocantinensis* endured an extended period of slow bone recycling with secondary osteons. Therefore, our study suggests that the metabolic shift leading to a higher growth rate among titanosauriforms possibly predated the origin of Titanosauria, perhaps occurring near the base of Somphospondyli, minimally at the common ancestor of *D. tocantinensis* and titanosaurs.

A previous study demonstrated different rates of secondary remodelling in the appendicular elements of the hadrosaur *Hypacrosaurus stebingeri* (Padian et al., 2016). Those authors hypothesized that secondary osteons might form to a greater degree in smaller bones (e.g. ulna, tibia), rather than in larger ones (e.g. humerus, femur). This difference in tissue profiles is the effect of the underlying metabolic mechanisms that aid these specific elements in achieving allometry throughout ontogeny. Higher secondary growth rates reduce vascularization, and consequently bone growth speed. Padian et al. (2016) suggested this mechanism should be present in all tetrapods and invited authors to test it in other taxa. Yet, the pattern seen in *D. tocantinensis* is quite the opposite (Figs 13–15). The femur is larger than the tibia, but has higher secondary remodelling, whereas the tibia still bears remnants of primary vascularization. The reasons why the smaller element is still growing at larger rates are unknown but indicate that related patterns may be more taxon-specific than suggested by Padian et al. (2016). A likewise higher growth rate for the tibia relative to the femur has been reported in a histovariability-controlled study of the crocodyliform *Pissarrachampsa sera* (Aureliano et al., 2025). Notably, this pattern is best interpreted as a taxon-specific adaptation, rather than a plesiomorphic feature of Archosauria, as it is not mirrored in extant crocodilian clades, in which the femur exhibits a slightly higher growth rate than the tibia (Eugenia et al., 2025; Woodward et al., 2014).

The use of ribs for skeletochronology has become progressively more common for extinct archosaurs, in order to avoid cutting more taxonomically informative elements (e.g. Brum et al., 2022; Windholz & Cerda, 2021). However, histovariability-controlled studies demonstrated inconsistencies between signatures present in ribs and appendicular bones (Farias, Carlisbino, et al., 2024; Farias, Desojo, et al., 2024; Klein et al., 2017), as expected to occur between different bones of the skeleton. Both the non-preservation of EFS and the excessive secondary remodelling in the sampled rib of *D. tocantinensis* differ from the histological signatures of its femur and tibia, supporting the notion that ribs alone are not adequate for ontogenetic estimates. Broader investigations on rib samples – with position control along the axial series and within each element – are necessary to show if these elements alone could be reliable for palaeohistology.

Biogeography

The inferred ancestral range of the clade formed by the *Ga. morellensis* plus *D. tocantinensis* lineage and its sister group, as including most continental areas of the earliest Cretaceous, fits palaeogeographical reconstructions that show a still coherent Laurasia barely separated from Gondwana at the time (Poropat et al., 2016; Scotese, 2021; Upchurch & Chiarenza, 2024). As for the *D. tocantinensis* plus *Ga. morellensis* dichotomy, age inferences younger than the Barremian do not fit the record of the latter taxon in that stage, so that a Valanginian–Barremian age is more likely as the clade origin. Further, its European origin reveals that the lineage including *D. tocantinensis* would have dispersed towards South America sometime between the Valanginian and Aptian. During the Early Cretaceous, likely connections between northern South America and

Europe were all via northern Africa. The South America to Africa land connection seems to have minimally lasted until the Albian (Granot & Dyment, 2015; Krause et al., 2019; Upchurch & Chiarenza, 2024), so that this would not be a dispersal problem. Yet, their connection to the European archipelago, including Iberia, was more erratic (Csiki-Sava et al., 2015; Dal Sasso et al., 2016; Holwerda et al., 2018), possibly suggesting an earlier dispersal from that original area. This scenario fits neatly with the 'Eurogondwanan hypothesis' of Ezcurra and Agnolín (2012), in which the European archipelago maintained a close connection to Gondwanan areas at least until the Hauterivian, allowing biotic interchanges. In fact, the 'Apulian route' (Bosellini, 2002) has been proposed to provide a later Africa–Europe connection during the Barremian–Aptian (Canudo et al., 2008). So, the Europe to Africa dispersion of the *D. tocantinensis* lineage could have happened via that route or perhaps earlier, following sea-level falls of the Mediterranean-Tethys during the Berriasian–Hauterivian (Miller et al., 2005).

Although Euhelopodidae and Titanosauria prevail in Asia and South America, respectively, the latter group experienced a broader early distribution (D'Emic, 2012), but with Lithostrotia usually considered more of a Gondwanan clade (Carballido, Otero, et al., 2022). Yet, Asia and Europe also appeared in some of its ancestral range reconstructions, presumably due to the nesting of *Normanniasaurus genceyi*, from the Albian of France, and the Chinese *Dongyangosaurus sinensis* and *Jiangshanosaurus lixianensis*, both from the Turonian-Coniacian Jinhua Formation, in the clade. Yet, the inclusion of these taxa among lithostrotians is controversial (Averianov & Sues, 2017; Le Loeuff et al., 2013; Mannion, Upchurch, Jin, et al., 2019); if they are not included, a strictly Gondwanan ancestral range would clearly be reconstructed for the group. As for other non-Gondwanan lithostrotians such as *A. sanjuanensis*, *Nemegtosaurus mongoliensis* and *Opisthocoelicaudia skarzynskii*, these are all latest Cretaceous in age and nested within clades with ancestral ranges reconstructed to South America (see Supplemental material). Hence, they most probably represent dispersal events from that continent to Laurasian areas, following the short-term establishment of the Panamanian Isthmus during the Campanian (Gorscak & O'Connor, 2016; Upchurch & Chiarenza, 2024).

Conclusions

The sauropod material unearthed from Davinópolis (Itapecuru Formation, Aptian), north-eastern Brazil, shares several traits with the European somphospondyl *Ga. morellensis*, but also bears differential traits supporting the establishment of new species *D. tocantinensis*. It exhibits notable histological traits, indicative of a growth pattern intermediate between those of early diverging titanosauriforms and highly nested titanosaurs. The new species not only expands our knowledge about the Early Cretaceous Titanosauriformes of northern South America but also reinforces the biogeographical connections between that part of the continent with more northern areas of Gondwana, as well as the European archipelago. In fact, numerical biogeography analyses suggest that the *Ga. morellensis* plus *D. tocantinensis* clade had a European origin, with the *D. tocantinensis* lineage dispensing via northern Africa to South America at some point between the Valanginian and Aptian. This finding also highlights that further research in the Early Cretaceous beds of north-eastern Brazil has the potential to enhance our understanding of sauropod evolution and palaeobiology.

Acknowledgements

We thank the 'Brado Logística' team, Carlos Eduardo Levy (Master Ambiental), Jardel Stênio de Araújo Barbosa, Paula Rocha Marino de Araújo, Geifance Abreu Santos, Amanda Almeida Cardoso, and Daniel Ribeiro da Silva (Arqueologística) for providing logistical support and assisting with the excavation; the latter for also first recognizing the fossils and alerting their supervisors. We also thank Giovani de Toledo Viecili (AMAI Fotografia) for photographical and audiovisual documentation of the excavation, Dr Ismar Carvalho for his assistance with the geology of the Itapecuru Formation, the colleagues from Instituto de Estudos do Xingu, UNIFESSPA, for providing support in the preparation and analysis of the fossils, and all the volunteers who helped with fossil preparation. We thank the Agência Nacional de Mineração for providing permissions and the Brazilian agencies FAPESP (20/07997-4 to MCL; 22/14694-3 to JCGSJ; 23/11098-3 to BAN; 24/09825-7 to PLG), CNPq (311140/2022-0 to JCC; 150635/2024-9 to KLNM), FUNPEC-UFRN (PIB21712-2023 to AMG), and FUNCAP/FPD (0213-00295.01.01/23 to TA) for financial support.

Disclosure statement

No potential conflict of interest was reported by the author(s).

Supplemental material

Supplemental material for this article can be accessed online here: https://doi.org/10.1080/14772019.2025.2601579.

ORCID

Elver L. Mayer http://orcid.org/0000-0002-0597-0773
Julian C. G. Silva Junior http://orcid.org/0000-0002-3389-7331
Leonardo R. Kerber http://orcid.org/0000-0001-8139-1493
Bruno A. Navarro http://orcid.org/0000-0002-0528-5389
Kamila L. N. Bandeira http://orcid.org/0000-0002-2744-8126
Juan C. Cisneros http://orcid.org/0000-0001-6159-1981
Manuel A. Medeiros http://orcid.org/0000-0003-3418-4736
Rafael M. Lindoso http://orcid.org/0000-0001-9100-2244
Aline M. Ghilardi http://orcid.org/0000-0001-9136-0236
Tito Aureliano http://orcid.org/0000-0002-6918-0519
Pedro L. Godoy http://orcid.org/0000-0003-4519-5094
Gabriel S. Ferreira http://orcid.org/0000-0003-1554-8346
Max C. Langer http://orcid.org/0000-0003-1009-4605

Data availability

The datasets that support the findings of this study are openly available through OSF at https://doi.org/10.17605/OSF.IO/KH5CV (Godoy, 2025) and MorphoSource at https://doi.org/10.17602/M2/M796733 (Aureliano, 2025).

References

Akaike, H. (1974). A new look at the statistical model identification. *IEEE Transactions on Automatic Control*, *19*, 716–723. https://doi.org/10.1109/TAC.1974.1100705

Almeida, F. F. M. (1977). O cráton do São Francisco. *Revista Brasileira de Geociências*, *7*, 349–364.

Almeida, F. F. M., **Hasui, Y.**, **Brito Neves, B. B.**, & **Fuck, R. A.** (1981). Brazilian structural provinces: an introduction. *Earth-Science Reviews*, *17*, 1–29.

Anaisse Júnior, J., **Truckenbrodt, W.**, & **Rossetti D. F.** (2001). Fácies de um sistema estuarino-lagunar no Grupo Itapecuru, área de Açailândia/MA, Bacia do Grajaú. In: **D. F. Rossetti**, **A. M. Góes** & **W. Truckenbrodt** (Eds.), *O Cretáceo na Bacia de São Luís-Grajaú* (pp. 119–150). Editora Museu Paraense Emílio Goeldi Friedrich Katzer.

Antonioli, L. (2001). *Estudo palino-cronoestratigráfico da Formação Codó-Cretáceo Inferior do nordeste brasileiro* [PhD thesis]. Programa de Pós-graduação em Geologia, Universidade Federal do Rio de Janeiro.

Apesteguía, S. (2005). Evolution of the titanosaur metacarpus. In: V. Tidwell & K. Carpenter (Eds.), *Thunder-lizards: The sauropodomorph dinosaurs* (pp. 321–345). Indiana University Press, Bloomington.

Arcanjo, S. H., **Sousa, D. V. B. A.**, **Medeiros, M. A.**, **Lindoso, R. M.**, **Sousa E. P.**, & **Carvalho, I. S.** (2023). Tectonic aspects of the Rio Parnaíba Lineament, duque Bacelar region, Maranhão State, based on the record of Dinosauria, Spinosaurinae. *Revista Brasileira de Paleontologia*, *26*, 114–121. https://doi.org/10.4072/rbp.2023.2.03

Aureliano, T. (2025). Media 000796733: Tibia [Dataset]. *MorphoSource*. https://doi.org/10.17602/M2/M796733

Aureliano, T., **Maciel, V.**, **Buck, P. V.**, **Montefeltro, F. C.**, **Marinho, T. D. S.**, & **Ghilardi, A. M.** (2025). Histovariability and fossil diagenesis of *Pissarrachampsa* (Pseudosuchia, Notosuchia, Baurusuchidae) from the Upper Cretaceous of Southeast Brazil. *The Anatomical Record*, *2025*, 1–13. https://doi.org/10.1002/ar.70021

Averianov, A, & **Sues, H.-D.** (2017). Review of Cretaceous sauropod dinosaurs from Central Asia. *Cretaceous Research*, *69*, 184. https://doi.org/10.1016/j.cretres.2016.09.006

Bandeira, K. L., **Navarro, B. A.**, **Pêgas, R. V.**, **Brilhante, N. S.**, **Brum, A. S.**, **de Souza, L. G.** & **Gallo, V.** (2024). A reassessment of the historical fossil findings from Bahia State (Northeast Brazil) reveals a diversified dinosaur fauna in the Lower Cretaceous of South America. *Historical Biology*, *37*, 548–589. https://doi.org/10.1080/08912963.2024.2318406

Bapst, D. W. (2012). Paleotree: an R package for paleontological and phylogenetic analyses of evolution. *Methods in Ecology and Evolution*, *3*, 803–807. https://doi.org/10.1111/j.2041-210X.2012.00223.x

Bapst, D. W. (2013). A stochastic rate-calibrated method for time-scaling phylogenies of fossil taxa. *Methods in Ecology and Evolution*, *4*, 724–733. https://doi.org/10.1111/2041-210X.12081

Bapst, D. W. (2014). Assessing the effect of time-scaling methods on phylogeny-based analyses in the fossil record. *Paleobiology*, *40*, 331–351. https://doi.org/10.1666/13033

Bapst, D. W., & **Hopkins, M. J.** (2017) Comparing cal3 and other a posteriori time-scaling approaches in a case study with the pterocephaliid trilobites. *Paleobiology*, *43*, 49–67. https://doi.org/10.1017/pab.2016.34

Batista, D. L., **Carvalho, I. S**, & **De la Fuente, M. S.** (2021). A new Cretaceous (Pleurodira: Pelomedusoides) from the Lower Cretaceous of Parnaíba Basin, Brazil. *Journal of South American Earth Sciences*, *105*, 102872. https://doi.org/10.1016/j.jsames.2020.102872

Bellardini, F., **Coria, R. A.**, **Pino, D. A.**, **Windholz, G. J.**, **Baiano, M. A.**, & **Martinelli, A. G.** (2022). Osteology and phylogenetic relationships of *Ligabuesaurus leanzai* (Dinosauria: Sauropoda) from the Early Cretaceous of the Neuquén Basin, Patagonia, Argentina. *Zoological Journal of the Linnean Society*, *196*, 1333–1393. https://doi.org/10.1093/zoolinnean/zlac003

Bonaparte, J. F. (1986). The dinosaurs (Carnosaurs, Allosaurids, Sauropods, Cetiosaurids) of the Middle Jurassic of Cerro Cóndor (Chubut, Argentina). *Annales de Paléontologie*, *72*, 325–386.

Bonaparte, J. F., Heinrich, W.-D., & Wild, R. (2000). Review of *Janenschia* Wild, with the description of a new sauropod from the Tendaguru beds of Tanzania and a discussion on the systematic value of procoelous caudal vertebrae in the Sauropoda. *Palaeontographica, Abteilung A*, **256**, 25–76. https://doi.org/10.1127/pala/256/2000/25

Bonaparte, J. F., González Riga, B. J., & Apesteguía, S. (2006). *Ligabuesaurus leanzai* gen. et sp. nov. (Dinosauria, Sauropoda), a new titanosaur from the Lohan Cura Formation (Aptian, Lower Cretaceous) of Neuquén, Patagonia, Argentina. *Cretaceous Research*, *27*, 364–376. https://doi.org/10.1016/j.cretres.2005.07.004

Bosellini, A. (2002). Dinosaurs "re-write" the geodynamics of the eastern Mediterranean and the paleogeography of the Apulia Platform. *Earth-Science Reviews*, *59*, 211–234. https://doi.org/10.1016/S0012-8252(02)00075-2

Brum, A. S., Bandeira, K. L. N., Sayão, J. M., Campos, D. A., & Kellner, A. W. A. (2022). Microstructure of axial bones of lithostrotian titanosaurs (Neosauropoda: Sauropodomorpha) shows extended fast-growing phase. *Cretaceous Research*, *136*, 105220. https://doi.org/10.1016/j.cretres.2022.105220

Campbell, D. F. (1949). *Revised report on the reconnaissance geology of the Maranhão Basin*. Petrobras, Rept 7, RENOR 93, Relatório Interno, Belém.

Cantino, P. D., & De Queiroz, K. (2020). *PhyloCode: a phylogenetic code of biological nomenclature*. CRC Press.

Canudo, J. I., Royo-Torres, R., & Cuenca-Bescós, G. (2008). A new sauropod: *Tastavinsaurus sanzi* gen. et sp. nov. from the Early Cretaceous (Aptian) of Spain. *Journal of Vertebrate Paleontology*, *28*, 712–731. https://doi.org/10.1671/0272-4634(2008)28[712:ANSTSG]2.0.CO;2

Carballido, J. L., Bellardini, F., & Salgado, L. (2022). The rise of non-titanosaur macronarians in South America. In: A. Otero, J. L. Carballido & D. Pol (Eds,), *South American Sauropodomorph Dinosaurs* (pp. 237–268). Springer Earth System Sciences. Springer. https://doi.org/10.1007/978-3-030-95959-3_7

Carballido, J. L., Otero, A., Mannion, P. D., Salgado, L., & A. Pérez Moreno. (2022). Titanosauria: a critical reappraisal of its systematics and the relevance of the South American Record. In: A. Otero, J. L. Carballido & D. Pol (Eds.), *South American Sauropodomorph Dinosaurs* (pp. 269–298). Springer Earth System Sciences. Springer. https://doi.org/10.1007/978-3-030-95959-3_8

Carballido, J. L., Pol, D., Cerda, I., & Salgado, L. (2011). The osteology of *Chubutisaurus insignis* Del Corro, 1975 (Dinosauria: Neosauropoda) from the 'Middle' Cretaceous of Central Patagonia, Argentina. *Journal of Vertebrate Paleontology*, *31*, 93–110. https://doi.org/10.1080/02724634.2011.539651

Carvalho, I. S. (1994). *Candidodon*: um crocodilo com heterodontia (Notosuchia, Cretáceo Inferior – Brasil). *Anais da Academia Brasileira de Ciências*, *66*, 331–346.

Carvalho, I. S. (2004). Dinosaur footprints from northeastern Brazil: taphonomy and environmental setting. *Ichnos*, *11*, 311–321. https://doi.org/10.1080/10420940490442368

Carvalho, I. S., Avilla, L. S., & Salgado, L. (2003). *Amazonsaurus maranhensis* gen. et sp. nov. (Sauropoda, Diplodocoidea) from the Lower Cretaceous (Aptian–Albian) of Brazil. *Cretaceous Research*, *24*, 697–713.

Carvalho, I. S., Salgado, L., Lindoso, R. M., Araújo-Júnior, H. I., Nogueira, F. C. C., & Soares, J. A. (2017). A new basal titanosaur (Dinosauria, Sauropoda) from the Lower Cretaceous of Brazil. *Journal of South American Earth Sciences*, *75*, 74–84. https://doi.org/10.1016/j.jsames.2017.01.010

Castro, D. F., Bertini, R. J., Santucci, R. M., & Medeiros, M. A. (2007). Sauropods of the Itapecuru Group (Lower/Middle Albian), São Luís-Grajaú Basin, Maranhão state, Brazil. *Revista Brasileira de Paleontologia*, *10*, 195–200. https://doi.org/10.4072/rbp.2007.3.06

Chure, D., Britt, B. B., Whitlock, J. A., & Wilson, J. A. (2010). First complete sauropod dinosaur skull from the Cretaceous of the Americas and the evolution of sauropod dentition. *Naturwissenschaften*, *97*, 379–391. https://doi.org/10.1007/s00114-010-0650-6

Corrêa-Martins, F. J. (2019). The neostratotype of Itapecuru Formation (Lower-middle Albian) and its impact for mesozoic stratigraphy of Parnaíba Basin. *Anais da Academia Brasileira de Ciências*, *91*, 1–19. https://doi.org/10.1590/0001-3765201920180730

Costa Neto, M. C. D., Lopes, E. C. D. S., Anjos, G. C. D., & Melo, A. F. F. D. (2014). *Geologia da Folha Imperatriz–SB. 23-VCV, Estado do Maranhão, Escala 1: 100.000*. CPRM, Serviço Geológico do Brasil. 87 pp.

Cruzado-Caballero, P., Filippi, L. S., González-Dionis, J., & Canudo, J. I. (2023). How common are lesions on the tails of sauropods? Two new pathologies in titanosaurs from the Late Cretaceous of Argentine Patagonia. *Diversity*, *15*, 464. https://doi.org/10.3390/d15030464

Csiki-Sava, Z., Buffetaut, E., Ősi, A., Pereda-Suberbiola, X., & Brusatte, S. L. (2015). Island life in the Cretaceous-faunal composition, biogeography, evolution, and extinction of land-living vertebrates on the Late Cretaceous European archipelago. *ZooKeys*, *469*, 1–161. https://doi.org/10.3897/zookeys.469.8439

Curry-Rogers, K., & Forster, C. A. (2001). The last of the dinosaur titans: a new sauropod from Madagascar. *Nature*, *412*(6846), 530–534.

Curry-Rogers, K., & Kulik, Z. (2018). Osteohistology of *Rapetosaurus krausei* (Sauropoda: Titanosauria) from the Upper Cretaceous of Madagascar. *Journal of Vertebrate Paleontology*, *38*, 1–24.

Dal Sasso, C., Pierangelini, G., Famiani, F., Cau, A., & Nicosia, U. (2016). First sauropod bones from Italy offer new insights on the radiation of Titanosauria between Africa and Europe. *Cretaceous Research*, *64*, 88–109. https://doi.org/10.1016/j.cretres.2016.03.008

D'Emic, M. D. (2012). Revision of the sauropod dinosaurs of the Lower Cretaceous Trinity Group, southern USA, with the description of a new genus. *Journal of Systematic Palaeontology*, *11*, 707–726. https://doi.org/10.1080/14772019.2012.667446

Díez Díaz, V., Demuth, O. E., Schwarz, D., & Mallison, H. (2020). The tail of the Late Jurassic sauropod *Giraffatitan brancai*: Digital reconstruction of its epaxial and hypaxial musculature, and implications for tail biomechanics. *Frontiers in Earth Science*, *8*, 160. https://doi.org/10.3389/feart.2020.00160

Eugenia, P. M., Bona, P., Siroski, P., & Chinsamy, A. (2025). Analyzing the life history of caimans: The growth dynamics of *Caiman latirostris* from an osteohistological

approach. *Journal of Morphology*, *286*, e70010. https://doi.org/10.1002/jmor.70010

Ezcurra, M. D., & **Agnolín, F. L.** (2012). A new global palaeobiogeographical model for the Late Mesozoic and Early Tertiary. *Systematic Biology*, *61*, 553–566. https://doi.org/10.1093/sysbio/syr115

Farias, B. D. M., **Carlisbino, T.**, **Mastrantonio, B. M.**, **Desojo, J. B.**, **Schultz, C. L.**, & **Soares, M. B.** (2024). The first ontogenetic model for non-crocodylomorph loricatans, based on osteohistology of the ontogenetic series of *Prestosuchus chiniquensis* from the Middle Triassic of Brazil. *The Anatomical Record*, *308*, 598–628.

Farias, B. D. M., **Desojo, J. B.**, **Cerda, I. A.**, **Ribeiro, A. M.**, **Ferigolo, J.**, **Carlisbino, T.**, **Schultz, C. L.**, **Mastrantonio, B. M.**, & **Soares M. B.** (2024). Bone histology supports gregarious behavior and an early ontogenetic stage to *Decuriasuchus quartacolonia* (Pseudosuchia: Loricata) from the Middle-Late Triassic of Brazil. *The Anatomical Record*, *307*, 957–973.

Ferreira, N. N, **Ferreira, E. P.**, **Ramos, R. R. C.**, & **Carvalho, I. S.** (2016). Palynological and sedimentary analysis of the Igarapé Ipiranga and Querru 1 outcrops of the Itapecuru Formation (Lower Cretaceous, Parnaíba Basin), Brazil. *Journal of South American Earth Sciences*, *66*, 15–31. https://doi.org/10.1016/j.jsames.2015.12.005

Ferreira, N. N., **Ferreira, E. P.**, **Ramos, R. R. C.**, & **Carvalho, I. S.** (2020). Terrestrial and marine palynomorphs from deposits of the pull-apart rift of West Gondwana (Parnaíba Basin, northern Brazil): Biostratigraphy and relation to tectonic events. *Journal of South American Earth Sciences*, *101*, 102612. https://doi.org/10.1016/j.jsames.2020.102612

Ferreira, N. N., **Ramos, R. R. C.**, **Ferreira, E. P.**, & **Carvalho, I. S.** (2021). Lithofaciological analysis of the exposed rocks of the Itapecuru Formation, northeastern Parnaíba Basin, Brazil: paleoenvironmental implications. *Journal of South American Earth Sciences*, *107*, 103114. https://doi.org/10.1016/j.jsames.2020.103114

França, T. C., **Brilhante, N. S.**, **Delcourt, R.**, **Silva, J. L.**, **Hendrickx, C.**, **Medeiros, M. A.**, & **Costa, F. R.** (2025). A carcharodontosaurid tooth from "Boca de Forno" Ravine of the Itapecuru Formation, Parnaíba Basin, Maranhão, Brazil. *Cretaceous Research*, *175*, 106163. https://doi.org/10.1016/j.cretres.2025.106163

Francillon-Viellot, H., **de Buffrénil, V.**, **Castanet, J.**, **Géraudie, J.**, **Meunier, F. J.**, **Sire, J. Y.**, **Zylberberg, L.**, & **de Ricqlès A.** (1990). Microstructure and mineralization of vertebrate skeletal tissues. In: J. Carter (Ed.), *Skeletal Biomineralization: Patterns, Processes and Evolutionary Trends* (pp. 473–530). Short Courses in Geology, Volume **5**, American Geophysical Union.

Ghilardi, A. M., **Aureliano, T.**, **Duque, R. R.**, **Fernandes, M. A.**, **Barreto, A. M.**, & **Chinsamy, A.** (2016). A new titanosaur from the Lower Cretaceous of Brazil. *Cretaceous Research*, *67*, 16–24. https://doi.org/10.1016/j.cretres.2016.07.001

Gilmore, C. W. (1925). A nearly complete articulated skeleton of *Camarasaurus*: A saurischian dinosaur from the Dinosaur National Monument, Utah. *Memoirs of the Carnegie Museum*, *10*(3), 347–410. https://doi.org/10.5962/p.217807

Godoy, P. L. (2025). Data for "A new titanosauriform with European affinities in the Early Cretaceous of Brazil: insights on Somphospondyli phylogeny, histology, and biogeography" [dataset]. *OSF*. https://doi.org/10.17605/OSF.IO/KH5CV

Godoy, P. L., **Cidade, G. M.**, **Montefeltro, F. C.**, **Langer, M. C.**, & **Norell, M. A.** (2020). Redescription and phylogenetic affinities of the caimanine *Eocaiman cavernensis* (Crocodylia, Alligatoroidea) from the Eocene of Argentina. *Papers in Palaeontology*, *7*, 1205–1231. https://doi.org/10.1002/spp2.1339

Góes, A. M. (1995). *Formação Poti (Carbonífero Inferior) da Bacia do Parnaíba* [PhD thesis]. Instituto de Geociências, Universidade de São Paulo.

Góes, A. M., & **Coimbra, A. M.** (1996). Bacias sedimentares da província sedimentar do meio-norte do Brasil. *V Simpósio de Geologia da Amazônia*. *Boletim de Resumos Expandidos e Guia de Excursões*, **1**, 186–187.

Góes, A. M., & **Rossetti, D. F.** (2001). Gênese da Bacia de São Luís-Grajaú, Meio-Norte do Brasil. In: **D. F. Rossetti**, **A. M. Góes** & **W. Truckenbrodt** (Eds.), *O Cretáceo na Bacia de São Luís-Grajaú* (pp. 15–29). Editora Museu Paraense Emílio Goeldi Friedrich Katzer.

Goloboff, P. A., & **Catalano, S. A.** (2016). TNT version 1.5, including a full implementation of phylogenetic morphometrics. *Cladistics*, *32*, 221–238. https://doi.org/10.1111/cla.12160

Gomes, Z. T., **Erickson, R. F.**, **Aureliano, T.**, & **Ghilardi, A. M.** (2024). A new ichnosite and ichnogenus from the Lower Cretaceous Rio do Peixe Basin, Brazil, with novel insights into the evolution of Titanosauriformes. *Historical Biology*, *37*(8), 1780–1794. https://doi.org/10.1080/08912963.2024.2385613

Gonçalves, R. A., & **Carvalho, I. S.** (1996). Contribuição ao estudo da sedimentação da Formação Itapecuru – região de Itapecuru-Mirim, Bacia do Parnaíba (Cretáceo Inferior) – Maranhão – Brasil. *Revista de Geología*, **9**, 75–81.

González Riga, B. J., **Calvo, J. O.**, & **Porfiri, J.** (2008). An articulated titanosaur from Patagonia (Argentina): new evidence of neosauropod pedal evolution. *Palaeoworld*, *17*, 33–40. https://doi.org/10.1016/j.palwor.2007.08.003

González Riga, B. J., **Casal, G. A.**, **Fiorillo, A. R.**, & **Ortiz David, L. D.** (2022). Taphonomy: overview and new perspectives related to the paleobiology of giants. In: A. Otero, J. L. Carballido & D. Pol (Org.). *South American Sauropodomorph Dinosaurs: Record, Diversity and Evolution* (pp. 541–582). Springer. https://doi.org/10.1007/978-3-030-95959-3_15

Gorscak E., & **O'Connor, P. M.** (2016). Time calibrated models support congruency between Cretaceous continental rifting and titanosaurian evolutionary history. *Biological Letters*, *12*, 20151047. https://doi.org/10.1098/rsbl.2015.1047

Granot R, & **Dyment J.** (2015). The Cretaceous opening of the South Atlantic Ocean. *Earth and Planetary Science Letters*, *414*, 156–163. https://doi.org/10.1016/j.epsl.2015.01.015

Guerra-Sommer, M., **Degani-Schmidt, I.**, **Mendonça, J. O.**, **Mendonça Filho, J. G.**, **Lopes, F. D. S.**, **Salgado-Campos, V. M. J.**, **Araújo, B.**, & **Carvalho, I. S.** (2021). Multidisciplinary approach as a key for paleoenvironmental interpretation in a *Weichselia*-dominant interval from the late Aptian Codó Formation (Parnaíba Basin, Brazil). *Journal of South American Earth Sciences*, *111*, 103490. https://doi.org/10.1016/j.jsames.2021.103490

Hedrick, B. (2012). Bone microstructure and relative age of the holotype specimen of the diplodocoid sauropod dinosaur *Suuwassea emilieae*. *Acta Palaeontologica Polonica*, **59**, 295–304. https://doi.org/10.4202/app.2012.0049

Holwerda, F. M., **Díez Díaz, V.**, **Blanco, A.**, **Montie, R.**, & **Reumer, J. W. F.** (2018). Late Cretaceous sauropod tooth morphotypes may provide supporting evidence for faunal connections between North Africa and Southern Europe. *PeerJ*, *6*, e5925. https://doi.org/10.7717/peerj.5925

Janensch, W. (1961). Die Gliedmaszen und Gliedmaszengürtel der Sauropoden der Tendaguru-Schichten. *Palaeontographica (Supplement 7)*, *3*, 177–235.

Klein, N., **Foth, C.**, & **Schoch, R. R.** (2017). Preliminary observations on the bone histology of the Middle Triassic pseudosuchian archosaur *Batrachotomus kupferzellensis* reveal fast growth with laminar fibrolamellar bone tissue. *Journal of Vertebrate Paleontology*, **37**, e1333121. https://doi.org/10.1080/02724634.2017.1333121

Klein, D. C., & **P. M. Sander.** (2008). Ontogenetic stages in the long bone histology of sauropod dinosaurs. *Paleobiology*, **34**, 247–263. https://doi.org/10.1666/0094-8373(2008)034[0247:OSITLB]2.0.CO;2

Klein, N., **Sander, P. M.**, **Stein, K.**, **Le Loeuff, J.**, **Carballido, J. L.**, & **Buffetaut, E.** (2012). Modified laminar bone in *Ampelosaurus atacis* and other Titanosaurs (Sauropoda): implications for life history and physiology. *PloS One*, **7**, e36907. https://doi.org/10.1371/journal.pone.0036907

Klein, E. L., & **Sousa, C. S.** (2012). *Geologia e Recursos Minerais do Estado do Maranhão*. CPRM, Serviço Geológico do Brasil.

Krause, D. W., **Sertich, J. J. W.**, **O'Connor, P. M.**, **Curry-Rogers, K**, & **Rogers, R. R.** (2019). The Mesozoic biogeographic history of Gondwanan terrestrial vertebrates: insights from Madagascar's fossil record. *Annual Review of Earth and Planetary Sciences*, *47*, 519–553. https://doi.org/10.1146/annurev-earth-053018-060051

Lacerda, L., **Bandeira, K. L.**, **Navarro, B. A.**, **Bertolossi, M. L.**, **Gallo, V.**, **da Silva, R. C.**, & **Kellner, A. W.** (2025). New lithostrotian specimens (Neosauropoda: Titanosauria) from the Mato Grosso State (western Brazil) and comments about tail injuries in sauropod dinosaurs. *Journal of South American Earth Sciences*, *153*, 105336. https://doi.org/10.1016/j.jsames.2024.105336

Lacovara, K. J., **Lamanna, M. C.**, **Ibiricu, L. M.**, **Poole, J. C.**, **Schroeter, E. R.**, **Ullmann, P. V.**, **Voegele, K. K.**, **Boles, Z. M.**, **Carter, A. M.**, **Fowler, E. K.**, **Egerton, V. M.**, **Moyer, A. E.**, **Coughenour, C. L.**, **Schein, J. P.**, **Harris, J. D.**, **Martínez, R. D.**, & **Novas, F. E.** (2014). A gigantic, exceptionally complete titanosaurian sauropod dinosaur from southern Patagonia, Argentina. *Scientific Reports*, *4*, 6196. https://doi.org/10.1038/srep06196

Landis, M. J., **Matzke, N. J.**, **Moore, B. R.**, & **Huelsenbeck, J.** (2013). Bayesian analysis of biogeography when the number of areas is large. *Systematic Biology*, **62**, 789–804. https://doi.org/10.1093/sysbio/syt040

Langer, M. C., **Delcourt, R.**, **Montefeltro, F. C.**, **Silva Junior, J. C. S.**, **Soler, M. G.**, **Ferreira, G. S.**, **Ruiz, J.**, **Barcelos, L.**, **Onary, S.**, **Marsola, J.**, **Castro, M.**, **Cidade, G.**, & **Batezelli, A.** (2022). The Bauru Basin in São Paulo and its Tetrapods. *Derbyana*, *43*, e776. https://doi.org/10.14295/derb.v43.776

Leite, J. F., **Aboarrage, A. M.**, & **Daemon, R. F.** (1975). *Projeto Carvão da Bacia do Parnaíba*. Companhia de Produção e de Recursos Minerais.

Le Loeuff, J., **Suteethorn, S.**, & **Buffetaut, E.** (2013). A new sauropod dinosaur from the Albian of Le Havre (Normandy, France). *Oryctos*, *10*, 23–30.

Leonardi, G. (1989). Inventory and statistics of the South American dinosaurian ichnofauna and its paleobiological interpretation. *International Symposium on Dinosaur Tracks and Traces*, *1*, 165–178.

Leonardi, G. (1994). Annotated atlas of South America tetrapod footprints (Devonian to Holocene) with an appendix on Mexico and Central America. CPRM, Serviço Geológico do Brasil. 248 pp.

Lima, H. P., **Aranha, L. G. F.**, & **Feijó, F. J.** (1994). Bacias de Bragança-Viseu, São Luís e Gráben de Ilha Nova. *Boletim de Geociências da Petrobrás*, *8*, 111–116.

Lindoso, R. M., & **Carvalho, I. S.** (2012). Crustáceos da Formação Codó (Bacia do Parnaíba, Brasil). In: F. C. Lopes, A. I. Andrade, M. H. Henriques, M. Quinta-Ferreira, M. T. Barata & R. Pena dos Reis (Org.). *Para conhecer a Terra: memórias e notícias de Geociências no espaço lusófono* (pp. 171–177). Universidade de Coimbra.

Lindoso, R. M., **Maisey, J. G.**, & **Carvalho, I. S.** (2016). Ichthyofauna from the Codó Formation, Lower Cretaceous (Aptian, Parnaíba Basin), Northeastern Brazil and their paleobiogeographical and paleoecological significance. *Palaeogeography, Palaeoclimatology, Palaeoecology*, *447*, 53–64. https://doi.org/10.1016/j.palaeo.2016.01.045

Lisboa, M. A. R. (1914). Permian geology of northern Brazil. *American Journal of Science*, *S 4-37*, 425–443. https://doi.org/10.2475/ajs.s4-37.221.425

Lloyd, G. T., **Bapst, D. W.**, **Friedman, M.**, & **Davis, K. E.** (2016). Probabilistic divergence time estimation without branch lengths: dating the origins of dinosaurs, avian flight and crown birds. *Biology Letters*, *12*, 20160609. https://doi.org/10.1098/rsbl.2016.0609

Mannion, P. D., **Upchurch, P.**, **Barnes, R. N.**, & **Mateus, O.** (2013). Osteology of the Late Jurassic Portuguese sauropod dinosaur *Lusotitan atalaiensis* (Macronaria) and the evolutionary history of basal titanosauriforms. *Zoological Journal of the Linnean Society*, *168*, 98–206. https://doi.org/10.1111/zoj.12029

Mannion, P. D., **Upchurch, P.**, **Jin, X.**, & **Zheng, W.** (2019). New information on the Cretaceous sauropod dinosaurs of Zhejiang Province, China: impact on Laurasian titanosauriform phylogeny and biogeography. *Royal Society Open Science*, *6*, 191057. https://doi.org/10.1098/rsos.191057

Mannion, P. D., **Upchurch, P.**, **Schwarz, D.**, & **Wings, O.** (2019). Taxonomic affinities of the putative titanosaurs from the Late Jurassic Tendaguru Formation of Tanzania: phylogenetic and biogeographic implications for eusauropod dinosaur evolution. *Zoological Journal of the Linnean Society*, *185*, 784–909. https://doi.org/10.1093/zoolinnean/zly068

Marsh, O. C. (1878). Principal characters of American Jurassic dinosaurs. *American Journal of Science*, *3*(95), 411–416. https://doi.org/10.2475/ajs.s3-16.95.411

Martínez, R. D., **Giménez, O.**, **Rodríguez, J.**, **Luna, M.**, & **Lamanna, M. C.** (2004). An articulated specimen of the basal titanosaurian (Dinosauria: Sauropoda) *Epachthosaurus sciuttoi* from the early Late Cretaceous Bajo Barreal Formation of Chubut province, Argentina.

Journal of vertebrate Paleontology, *24*, 107–120. https://doi.org/10.1671/9.1

Matzke, N. J. (2013). *BioGeoBEARS: BioGeography with Bayesian (and likelihood) evolutionary analysis in R Scripts*. R package, version 0.2.

Matzke, N. J. (2014) Model selection in historical biogeography reveals that founder-event speciation is a crucial process in island clades. *Systematic Biology*, *63*, 951–970. https://doi.org/10.1093/sysbio/syu056

Medeiros, M. A., **Lindoso, R. M.**, **Mendes, I. D.**, & **Carvalho, I. S.** (2014). The Cretaceous (Cenomanian) continental record of the Laje do Coringa flagstone (Alcântara Formation), northeastern South America. *Journal of South American Earth Sciences*, *53*, 50–58. https://doi.org/10.1016/j.jsames.2014.04.002

Mendes, M., & **Borghi, L.** (2004). Análise faciológica da Formação Codó (Cretáceo, Bacia do Parnaíba) em testemunhos de sondagem. In *3rd Congresso Brasileiro de P&D em Petróleo e Gás*, Online.

Merle, R., **Marzoli, A.**, **Bertrand, H.**, **Reisberg, L.**, **Verati, C.**, **Zimmermann, C.**, **Chiaradia, M.**, **Bellieni, G.**, & **Ernesto, M.** (2011). 40Ar/39Ar ages and Sr–Nd–Pb–Os geochemistry of CAMP tholeiites from Western Maranhão basin (NE Brazil). *Lithos*, *122*, 137–151. https://doi.org/10.1016/j.lithos.2010.12.010

Mesner, J. C., & **Wooldridge, L. C. P.** (1964). Maranhão Paleozoic basin and Cretaceous coastal basins, north Brazil. *Bulletin of the American Association of Petroleum Geologists*, *48*, 1475–1512.

Miller, K. G., **Kominz, M. A.**, **Browning, J. V.**, **Wright, J. D.**, **Mountain, G. S.**, **Katz, M. E.**, **Sugarman, P. J.**, **Cramer, B. S.**, **Christie-Blick, N.**, & **Pekar S. F.** (2005). The phanerozoic record of global sea-level change. *Science*, *310*, 1293–1298. https://doi.org/10.1126/science.1116412

Mitchell, J., & **Sander, P. M.** (2014). The three-front model: a developmental explanation of long bone diaphyseal histology of Sauropoda. *Biological Journal of the Linnean Society*, *112*, 765–781. https://doi.org/10.1111/bij.12324

Mo, J., **Ma, F.**, **Yu, Y.**, & **Xu, X.** (2023). A new titanosauriform sauropod with an unusual tail from the Lower Cretaceous of northeastern China. *Cretaceous Research*, *144*, 105449. https://doi.org/10.1016/j.cretres.2022.105449

Mocho, P., **Escaso, F.**, **Gasulla, J. M.**, **Galobart, À.**, **Poza, B.**, **Santos-Cubedo, A.** & **Ortega, F.** (2023). New sauropod dinosaur from the Lower Cretaceous of Morella (Spain) provides new insights on the evolutionary history of Iberian somphospondylan titanosauriforms. *Zoological Journal of the Linnean Society*, *201*, 214–268. https://doi.org/10.1093/zoolinnean/zlad124

Mocho, P., **Perez-Garcia, V. A.** (2022). New titanosaurian caudal remains provide insights on the sauropod diversity of the Haţeg Island (Romania) during the Late Cretaceous. *Historical Biology, 35*(10), 1881–1916. https://doi.org/10.1080/08912963.2022.2125807

Navarro, B. A., **Ghilardi, A. M.**, **Aureliano, T.**, **Díaz, V. D.**, **Bandeira, K. L. N.**, **Cattaruzzi, A. G. S.**, **Iori, F. V.**, **Martine, A. M.**, **Carvalho, A. B.**, **Anelli, L. E.**, **Fernandes, M. A.**, & **Zaher, H.** (2022). A new nanoid titanosaur (Dinosauria: Sauropoda) from the Upper Cretaceous of Brazil. *Ameghiniana*, *59*, 317–354. https://doi.org/10.5710/AMGH.25.08.2022.3477

Nogueira, E., **Yanai, A.**, **de Vasconcelos, S.**, **de Alencastro, G.** & **Fearnside, P.** (2018). Brazil's Amazonian protected areas as a bulwark against regional climate change. *Regional Environmental Change*, *18*, 573–579. https://doi.org/10.1007/s10113-017-1209-2

Padian, K., **Werning, S.**, & **Horner, J. R.** (2016). A hypothesis of differential secondary bone formation in dinosaurs. *Comptes Rendus Palevol*, *15*, 40–48. https://doi.org/10.1016/j.crpv.2015.03.002

Pedrão E., **Lima, H. P.**, **Makino, R. K.**, & **Barrilari, I. M. R.** (2002). Palinoestratigrafia e evolução ambiental da seção cretácea das bacias de Bragança-Viseu e São Luís (margem equatorial brasileira). *Acta Geologica Leopoldensia*, *25*, 21–39.

Pereira, P. V., **Bandeira, K. L.**, **Vidal, L. S.**, **Ribeiro, T. B.**, **Candeiro, C. R. D. A.**, & **Bergqvist, L. P.** (2024). A new sauropod species from north-western Brazil: biomechanics and the radiation of Titanosauria (Sauropoda: Somphospondyli). *Zoological Journal of the Linnean Society*, *202*, zlae054. https://doi.org/10.1093/zoolinnean/zlae054

Pessoa, V. C. O., & **Borghi, L.** (2005). Análise faciológica da Formação Itapecuru (Cretáceo, Bacia do Parnaíba) em testemunhos de sondagem. In *3rd Congresso Brasileiro de P&D em Petróleo e Gás*, Online

Poropat, S. F., **Kundrát, M.**, **Mannion, P. D.**, **Upchurch, P.**, **Tischler, T. R.**, & **Elliott, D. A.** (2021). Second specimen of the Late Cretaceous Australian sauropod dinosaur *Diamantinasaurus matildae* provides new anatomical information on the skull and neck of early titanosaurs. *Zoological Journal of the Linnean Society*, *192*, 610–674. https://doi.org/10.1093/zoolinnean/zlaa173

Poropat, S. F., **Mannion, P. D.**, **Rigby, S. L.**, **Duncan, R. J.**, **Pentland, A. H.**, **Bevitt, J. J.** & **Elliott, D. A.** (2023). A nearly complete skull of the sauropod dinosaur *Diamantinasaurus matildae* from the Upper Cretaceous Winton Formation of Australia and implications for the early evolution of titanosaurs. *Royal Society Open Science*, *10*, 221618. https://doi.org/10.1098/rsos.221618

Poropat, S. F., **Mannion, P. D.**, **Upchurch, P.**, **Hocknull, S. A.**, **Kear, B. P.**, **Kundrát, M.**, **Tischler, T. R.**, **Sloan, T.**, **Sinapius, G. H. K.**, **Elliott, J. A.**, & **Elliott, D. A.** (2016). New Australian sauropods shed light on Cretaceous dinosaur palaeobiogeography. *Scientific Reports*, *6*, 34467. https://doi.org/10.1038/srep34467

Ramos, M. I. F., **Rossetti, D. F.**, & **Paz, J. D. S.** (2006). Caracterização e significado paleoambiental da fauna de ostracodes da Formação Codó (Neoaptiano), leste da bacia de Grajaú, MA, Brasil. *Revista Brasileira de Paleontologia*, *9*, 339–348. https://doi.org/10.4072/rbp.2006.3.09

R Core Team. (2022). *R: a language and environment for statistical computing*. R Foundation for Statistical Computing, Vienna, Austria. http://www.R-project.org/

Ree, R. H. (2005). Detecting the historical signature of key innovations using stochastic models of character evolution and cladogenesis. *Evolution*, *59*, 257–265.

Ree, R. H., & **Smith, S. A.** (2008). Maximum likelihood inference of geographic range evolution by dispersal, local extinction, and cladogenesis. *Systematic Biology*, **57**, 4–14. https://doi.org/10.1080/10635150701883881

Rezende, N. G. A. M. (2002). *A zona zeolítica da Formação Corda, Bacia do Parnaíba* [MSc dissertation]. Universidade Federal do Pará.

Ronquist, F. (1997). Dispersal-vicariance analysis: A new approach to the quantification of historical biogeography. *Systematic Biology*, **46**, 195–203. https://doi.org/10.1093/sysbio/46.1.195

Rose, P. J. (2007). A new titanosauriform sauropod (Dinosauria: Saurischia) from the Early Cretaceous of central Texas and its phylogenetic relationships. *Palaeontologia Electronica*, *10*, 8A.

Rossetti, D. F., Góes, A. M., & Arai, M. (2001). A passagem aptiano-albiano na Bacia do Grajaú, MA. In: D. F. Rossetti, A. M. Góes & W. Truckenbrodt (Eds.), *O Cretáceo na Bacia de São Luís-Grajaú* (pp. 101–117). Editora Museu Paraense Emílio Goeldi Friedrich Katzer.

Rossetti, D. F., & Truckenbrodt, W. (1997). Revisão estratigráfica para os depósitos do Albiano-Terciário inferior (?) na Bacia de São Luís, Maranhão. *Boletim do Museu Paraense Emílio Goeldi, Série Ciências da Terra*, *9*, 29–41.

Royo-Torres, R., Alcalá, L., & Cobos, A. (2012). A new specimen of the Cretaceous sauropod Tastavinsaurus sanzi from El Castellar (Teruel, Spain), and a phylogenetic analysis of the Laurasiformes. *Cretaceous Research*, *34*, 61–83. https://doi.org/10.1016/j.cretres.2011.10.005

Salgado, L., Coria, R. A., & Calvo, J. O. (1997). Evolution of titanosaurid sauropods: Phytogenetic analysis based on the postcranial evidence. *Ameghiniana*, *34*, 3–32.

Sander, P. (2000). Longbone histology of the Tendaguru sauropods: implications for growth and biology. *Paleobiology*, **26**, 466–488. https://doi.org/10.1666/0094-8373(2000)026<0466:LHOTTS>2.0.CO;2

Sander, P. M., Mateus, O., Laven, T., & Knötschke, N. (2006). Bone histology indicates insular dwarfism in a new Late Jurassic sauropod dinosaur. *Nature*, *441*, 739–741. https://doi.org/10.1038/nature04633

Santos, M. E. C., & Carvalho, M. S. S. (2009). *Paleontologia das bacias do Parnaíba, Grajaú e São Luís*. CPRM, Serviço Geológico do Brasil. 215 pp.

Schwarz-Wings, D., Frey, E., & Martin, T. (2009). Reconstruction of the bracing system of the trunk and tail in hyposaurine dyrosaurids (Crocodylomorpha; Mesoeucrocodylia). *Journal of Vertebrate Paleontology*, *29*, 453–472. https://doi.org/10.1671/039.029.0228

Scotese, C. R. (2021). An atlas of Phanerozoic paleogeographic maps: the seas come in and the seas go out. *Annual Review of Earth and Planetary Sciences*, *49*, 679–728. https://doi.org/10.1146/annurev-earth-081320-064052

Silva, L. S. O. (2023). *Novos registros de Sauropoda para a formação Itapecuru (Cretáceo Inferior), Bacia do Parnaíba, nordeste do Brasil* [MSc dissertation]. Universidade Federal do Espirito Santo.

Silva Junior, J. C., Martinelli, A. G., Iori, F. V., Marinho, T. S., Hechenleitner, E. M., & Langer, M. C. (2022). Reassessment of *Aeolosaurus maximus*, a titanosaur dinosaur from the Late Cretaceous of Southeastern Brazil. *Historical Biology*, *34*, 403–411. https://doi.org/10.1080/08912963.2021.1920016

Słowiak, J., Szczygielski, T., Rothschild, B. M., & Surmik, D. (2021). Dinosaur senescence: a hadrosauroid with age-related diseases brings a new perspective of "old" dinosaurs. *Scientific Reports*, *11*, 11947. https://doi.org/10.1038/s41598-021-91366-1

Stein, K., Csiki, Z., Curry- Rogers, K., Weishampel, D. B., Redelstorff, R., Carbadillo, J. L., & Sander, P. M. (2010). Small body size and extreme cortical bone remodeling indicate phyletic dwarfism in *Magyarosaurus dacus* (Sauropoda: Titanosauria). *Proceedings of the National Academy of Sciences*, *107*, 9258–9263. https://doi.org/10.1073/pnas.1000781107

Stubbs, T. L., Pierce, S. E., Elsler, A., Anderson, P. S., Rayfield, E. J., & Benton, M. J. (2021). Ecological opportunity and the rise and fall of crocodylomorph evolutionary innovation. *Proceedings of the Royal Society B*, *288*, 20210069. https://doi.org/10.1098/rspb.2021.0069

Sugiura, N. (1978). Further analysis of the data by Akaike's information criterion and the finite corrections. *Communications in Statistics – Theory and Methods*, **7**, 13–26. https://doi.org/10.1080/03610927808827599

Tidwell, V., Carpenter, K., & Brooks, W. (1999). New sauropod from the Lower Cretaceous of Utah, USA. *Oryctos*, *2*, 21–37.

Tidwell, V., Carpenter, K. & Meyer, S. (2001). New Titanosauriform (Sauropoda) from the Poison Strip Member of the Cedar Mountain Formation (Lower Cretaceous), Utah. In: D. H. Tanke & K. Carpenter (Eds.), *Mesozoic Vertebrate Life* (pp. 139–165). Indiana University Press.

Upchurch, P., & Chiarenza, A. A. (2024). A brief review of non-avian dinosaur biogeography: state-of-the-art and prospectus. *Biology Letters*, *20*, 20240429. https://doi.org/10.1098/rsbl.2024.0429

Vaz, P. T., Rezende, N. G. A. M., Wanderley Filho, J. R. & Travassos, W. A. S. (2007). *Bacia do Parnaíba*. *Boletim de Geociencias da Petrobrás*, *15*, 253–263.

Voegele, K. K., Ullmann, P. V., Lamanna, M. C., & Lacovara, K. J. (2020). Myological reconstruction of the pelvic girdle and hind limb of the giant titanosaurian sauropod dinosaur *Dreadnoughtus schrani*. *Journal of Anatomy*, **238**, 576–597. https://doi.org/10.1111/joa.13334

Wilson, J. A. (1999). A nomenclature for vertebral laminae in sauropods and other saurischian dinosaurs. *Journal of Vertebrate Paleontology*, *19*, 639–653. https://doi.org/10.1080/02724634.1999.10011178

Wilson, J. A. (2012). New vertebral laminae and patterns of serial variation in vertebral laminae of sauropod dinosaurs. *Contributions from the Museum of Paleontology, University of Michigan*, *32*, 91–110.

Wilson, J. A., & Carrano, M. T. (1999). Titanosaurs and the origin of "wide-gauge" trackways: a biomechanical and systematic perspective on sauropod locomotion. *Paleobiology*, *25*, 252–267. https://doi.org/10.1017/S0094837300026543

Wilson, J. A., D'Emic, M. D., Ikejiri, T., Moacdieh, E. M., & Whitlock, J. A. (2011). A nomenclature for vertebral fossae in sauropods and other saurischian dinosaurs. *PloS One*, **6**(2), e17114. https://doi.org/10.1371/journal.pone.0017114

Wilson, J. A., & Sereno, P. C. (1998). Early evolution and higher-level phylogeny of sauropod dinosaurs. *Journal of Vertebrate Paleontology*, **18**(S2), 1–79. https://doi.org/10.1080/02724634.1998.10011115

Wilson, J. A., & Upchurch, P. (2003). A revision of Titanosaurus Lydekker (Dinosauria-Sauropoda), the first dinosaur genus with a 'Gondwanan' distribution. *Journal of Systematic Palaeontology*, **1**, 125–160. https://doi.org/10.1017/S1477201903001044

Windholz, G. J., & Cerda, I. A. (2021). Paleohistology of two dicraeosaurid dinosaurs (Sauropoda; Diplodocoidea) from La Amarga Formation (Barremian–Aptian, Lower

Cretaceous), Neuquén Basin, Argentina: Paleobiological implications. *Cretaceous Research*, *128*, 104965. https://doi.org/10.1016/j.cretres.2021.104965

Woodward, H. (2005). *Bone histology of the sauropod dinosaur Alamosaurus sanjuanensis from the Javelina Formation, Big Bend National Park, Texas* [MSc dissertation]. Texas Tech University.

Woodward, H. N., **Horner, J. R.**, & **Farlow, J. O.** (2014). Quantification of intraskeletal histovariability in *Alligator mississippiensis* and implications for vertebrate osteohistology. *PeerJ*, *2*, e422. https://doi.org/10.7717/peerj.422

You, H., **Feng, T.**, & **Zhexi, L.** (2003). A new basal titanosaur (Dinosauria: Sauropoda) from the Early Cretaceous of China. *Acta Geologica Sinica*, *77*, 424–429.

Zalán, P. V. (2007). Bacias de Bragança-Viseu, São Luís e Ilha Nova. *Boletim de Geociências da Petrobras*, *15*, 341–345.

Associate Editor: Dr Kimberley Chapelle